Transceptor NRT1.1 and Receptor-Kinase QSK1 Complex Controls PM H -ATPase Activity Under Low Nitrate

Zhe Zhu, Leonard Krall, Zhi Li, Lin Xi, Hongxiu Luo, Shalan Li, Mingjie He, Xiaolin Yang, Haitao Zan, Max Gilbert, et al.

Transceptor NRT1.1 and receptor-kinase QSK1 complex controls PM H^+-ATPase activity under low nitrate

Zhe Zhu[1#], Leonard Krall[1#*], Zhi Li[2#], Lin Xi[2#], Hongxiu Luo[2], Shalan Li[1], Mingjie He[2], Xiaolin Yang[1], Haitao Zan[1], Max Gilbert[2], Sven Gombos[2], Ting Wang[6], Benjamin Neuhäuser[3], Aurore Jacquot[4], Laurence Lejay[4], Jingbo Zhang[5], Junzhong Liu[1], Waltraud X. Schulze[2*] and Xu Na Wu[1*]

1 State Key Laboratory of Conservation and Utilization of Bio-Resources in Yunnan and Center for Life Science, School of Life Sciences, Yunnan University, 650500 Kunming, China

2 Department of Plant Systems Biology, University of Hohenheim, 70599 Stuttgart, Germany

3 Nutritional Crop Physiology, University of Hohenheim, 70599 Stuttgart, Germany

4 IPSiM, Univ Montpellier, CNRS, INRAE, Institut Agro, 34060, Montpellier, France

5 National Academy of Agriculture Green Development ,College of Resources and Environmental Sciences, China Agricultural University, Beijing 100193, China

6 Key Laboratory of Cell Proliferation and Regulation Biology of Ministry of Education, College of Life Science, Beijing Normal University, Beijing 100875, China.

*Corresponding Author:

Prof. Xu Na Wu (xwu@ynu.edu.cn)

Prof. Waltraud Schulze (wxschulze@uni-hohenheim.de)

Dr. Leonard Krall (lenkrall@gmail.com)

#Authors contribution equally

Keywords: membrane phosphoproteomics of *nrt1.1-1*, co-receptor kinase QSK1, PM-H^+-ATPase activity, low nitrate, apoplast acidification, lateral root growth

Running title: NRT1.1-RK complex controls proton pump activity in low nitrate

Summary

NRT1.1, a nitrate transceptor, plays an important role in nitrate binding, sensing and nitrate dependent lateral root (LR) morphology. However, little is known about NRT1.1-mediated nitrate signaling transduction through plasma membrane (PM)-localized proteins. Through in-depth phosphoproteome profiling using membranes of *Arabidopsis* roots, we identified receptor kinase QSK1 and plasma membrane H^+-ATPase AHA2 as potential downstream components of NRT1.1 signaling in a mild low nitrate (LN)-dependent manner. QSK1, as a functional kinase and molecular link, physically interacts with NRT1.1 and AHA2 at LN, and specifically phosphorylates AHA2 at S899. Importantly, we found that LN, not HN, induces formation of NRT1.1-QSK1-AHA2 complex in order to repress the proton efflux into the apoplast by increased phosphorylation of AHA2 at S899. Loss of either NRT1.1 or QSK1 thus results in a higher T947/S899 phosphorylation ratio on AHA2, leading to enhanced pump activity and longer LRs under LN. Our results uncover a regulatory mechanism in which NRT1.1, under LN conditions, recruits coreceptor QSK1 into a complex to transduce LN sensing to the PM H^+-ATPase AHA2, controlling the phosphorylation ratio of activating and inhibitory phosphorylation sites on AHA2. This then results in altered proton pump activity, apoplast acidification, and regulation of NRT1.1-mediated LR growth.

Introduction

Nitrogen is an essential macronutrient and nitrate serves as an important signaling molecule required for growth, gene expression, and metabolism in plants.[1] The nitrate concentration in soil can influence plant root growth, shoot elongation, as well as crop yield. Improving nitrate use efficiency in plants is critical for increasing agricultural production. The molecular mechanism of how nitrate is sensed and transported into plants is well known since the characterization of the nitrate transporter and sensor (transceptor) NRT1.1[2] (CHL1/NPF6.3) and the high-affinity nitrate transporter NRT2.1[3] in *Arabidopsis thaliana*.

NRT1.1 in *Arabidopsis* is essential for nitrate transport, sensing, binding and signaling.[4] Phosphorylation of NRT1.1 at T101 by the CIPK23-CBL9 calcium sensor-kinase complex switches NRT1.1 from a low-affinity to a high-affinity transporter and increases NRT1.1-dependent nitrate uptake.[5] Dephosphorylation of NRT1.1 is fine-tuned by protein phosphatase ABI2 (abscisic acid insensitive 2).[6] NRT1.1 activation also induces a rapid increase in cytoplasmic Ca^{2+} levels.[7] Recently, the NRT1.1-CNGC15 module was found to be a molecular switch that controls calcium influx in a nitrate-dependent manner.[8] Calcium subsequently activates CPK10/30/32 to phosphorylate transcription factor NLP7 at S205, promoting NLP7 retention in the nucleus.[9] Very recently, NLP7 was shown to be an intracellular nitrate sensor, as nitrate can bind NLP7 directly.[10] In rice, OsNRT1.1B-SPX4-NBIP-OsNLP3 was the first module that demonstrated nitrate signaling from the plasma membrane (PM) to the nucleus.[11] However, little is known about whether more regulatory components in NRT1.1-mediated nitrate signal transduction exist in the PM.

NRT1.1 also plays an important role in root morphology by directly influencing lateral root (LR) growth. Under low nitrate (LN) availability, NRT1.1 as well as phosphorylation of NRT1.1 at T101 plays a key role in repression of LR growth, and NRT1.1 is considered to repress LR growth through its auxin transport capacity.[12,13] Other studies also revealed that there is a crosstalk between nitrate and auxin in modulating of NRT1.1-dependent LR growth.[14] Plasma membrane-localized H^+-ATPases pump H^+ into the apoplast between the plasma membrane and cell wall, resulting in acidification of the apoplast and increased cell elongation.[15,16] However, it remains unknown

whether NRT1.1-mediated LR growth inhibition under LN relies on altered PM H^+-ATPase activity and apoplastic pH.

Many studies have suggested that genes involved in nitrate signaling are regulated at the transcriptional level.[17-19] However, there are indications of posttranslational regulation of nitrogen uptake, sensing, and metabolism through phosphorylation.[20] Numerous nitrogen-dependent phosphoproteomic studies[21-24] identified PM-localized transporters and receptor kinases, which showed nitrate-dependent phosphorylation changes. However, whether, and by which molecular mechanisms these PM proteins are involved in nitrate signaling and transport regulation still needs to be explored.

Here we carried out a systematic functional study of roots of WT and *nrt1.1-1* to generate mild low and high nitrate-induced membrane protein phosphorylation profiles. Using these profiles, we aimed to discover new regulatory components for NRT1.1-mediated nitrate signal transduction. Ultimately, we uncovered a novel function of NRT1.1, which interacts with the receptor kinase QSK1 to constitute a molecular switch that controls PM H^+-ATPase activity through phosphorylation balance on different phosphorylation sites (T947/S899) of AHA2 in a mild low nitrate dependent manner.

Results

Functional membrane phosphorylation profiling identifies downstream components of NRT1.1

We performed a comparative phosphoproteomic analysis of *Arabidopsis* root membrane protein comparing WT and *nrt1.1-1* under mild low nitrate (LN) and high nitrate (HN)-induced conditions after nitrogen starvation (NS) (Figure.1A) to identify downstream components that may be involved in NRT1.1-dependent LR growth and signal transduction. We identified 5,950 phosphosites corresponding to 1,945 proteins (Figure.S1A). Among these, there were 2,390 previously uncharacterized phosphosites and 3,246 new nitrate-induced phosphosites compared to the PhosPhAt4.0 database[25] and published nitrate-induced phosphosites in *Arabidopsis*, respectively[21-23] (Figure S1B and S1C). Among these were 2,295 phosphosites corresponding to 1,280 proteins with localization probability >0.75 (class I sites), which were used for quantitative statistical analysis (Supplementary Table 1). The phosphorylation sites distributed to peptides with 93.4% single, 6% double, and 0.6% triple or more phosphorylation (Figure S1D). Principal component analysis (PCA)

revealed a strong separation of WT under LN and HN along the first principal component, and data points for WT at LN and *nrt1.1-1* at LN separated along the second component. Data points for WT and *nrt1.1-1* at HN clustered tightly and showed no separation (Figure 1B).

We performed stringent pairwise comparison analysis for genotypes and treatments to separate LN and HN specific responses. In the WT, 642 phosphosites exhibited significantly different abundance between LN vs NS or HN vs NS. Of these, 579 and 36 phosphosites were specifically changed under LN and HN, respectively. 515 of 579 phosphosites exhibited a higher abundance under LN (Figure 1C). Overall, LN induced larger changes in the membrane phosphoproteome compared to HN. Subsequently, we compared the phosphoproteome of the WT and *nrt1.1-1*. Under LN, 661 phosphosites were found with altered abundance in *nrt1.1-1*, out of which 608 phosphosites showed significantly decreased phosphorylation in *nrt1.1-1* (Figure 1D). The asymmetry of the plots suggested that the absence of NRT1.1 had a strong impact on the membrane phosphoproteome under LN. Overlap of phosphosites with significantly changed phosphorylation in WT under LN vs. HN, and under LN in *nrt1.1-1* compared to WT identified 307 phosphosites corresponding to 231 proteins as candidates for being downstream regulators of NRT1.1 (Figure 1E), indicating LN-induced phosphorylation of these proteins is dependent on the presence of NRT1.1. These 231 proteins were enriched in functions of Signaling (bin30), Transport (bin34), RNA (bin27), and Cell (bin31), and were overrepresented with subcellular locations at the PM and in the N (nucleus) (Figure 1F).

We then ranked the phosphosites with significantly changed phosphorylation in *nrt1.1-1* under LN (based on *p* values) and highlighted phosphosites on 19 transport-related proteins (Figure S1E). Among the highly-ranked phosphorylation sites, T947 and S899 from the plasma membrane H^+–adenosine triphosphatase 2 (PM H^+-ATPase isoform, AHA2) were also identified (Figure S2A and S2B). AHA2 is the major proton pump in roots. These two residues were reported as resulting in activation (T947) and inactivation (S899) upon phosphorylation[26,27], and are located in the C-terminal autoinhibitory domain.[28] AHA2 is known to promote both lateral root and primary root growth under LN.[29] T947 and S899 in AHA2 exhibited significantly higher phosphorylation in WT in LN than in HN, and phosphorylation at both sites, but especially S899 was drastically decreased in *nrt1.1-1* under LN, but not HN (Figure 2A

and 2B). AHA2 protein abundances showed no change (Figure 2C). These results suggested that the presence of NRT1.1 is required for phosphorylation of AHA2 under LN. Since phosphorylation at T947 and S899 have contrasting effects on AHA2 activity, we used the ratio of T947 and S899 phosphorylation as an indication of the balance of AHA2 activity. Interestingly, the phosphorylation ratio of T947/S899 was significantly increased in WT at LN compared to HN, and an even more increased ratio was found in *nrt1.1-1* compared to WT under LN, while no difference was observed under HN (Figure 2D). This suggests that loss of NRT1.1 disrupted the balance of phosphorylation between T947 and S899 at LN due to a stronger reduction of phosphorylation at S899.

NRT1.1 represses proton efflux at LN

PM-localized ATPases fine-tunes proton efflux into the apoplast, resulting in apoplastic acidification. To assess whether NRT1.1 is required for H^+-ATPase activation under LN, we applied membrane-impermeable 8-hydroxypyrene-1,3,6-trisulfonic acid trisodium salt (HPTS) as a ratiometric fluorescent pH indicator for assessing changes in the apoplastic pH at cellular resolution in the LR elongation zone.[30] Two different forms of HPTS (protonated and deprotonated) were observed in two channels using a confocal microscope with excitation wavelengths of 405 nm and 488 nm, respectively. The ratiometric value (458/405) represents the apoplastic pH, and a high ratio represents a relatively high pH. The WT exhibited a lower pH in LN compared to HN. Moreover, an even lower pH was observed in *nrt1.1-1* under LN (Figure 2E and 2F), uncovering that the higher phosphorylation ratio of T947/S899 (Figure 2D) resulted in activation of H^+-ATPase in WT under LN compared to HN, and an even more increased activation of the H^+-ATPase in *nrt1.1-1* than in WT under LN. These results suggested that PM H^+-ATPases function downstream of NRT1.1, mediating the LN-induced proton efflux into the apoplast space. In turn, the phosphorylation ratio of T947/S899 controls the AHA2 activity.

As a result of enhanced proton pump activity, the average cortical cell length of LRs in the WT was longer under LN than HN, and an even longer cortical cell length was observed in *nrt1.1-1* under LN, but not under HN (Figure 2G and 2H). Consequently, WT displayed longer LR length under LN, and *nrt1.1-1* exhibited more enhanced LR growth (Figure S2C and S2D). Taken together, our results suggested that the lower

apoplastic pH in the LR elongation zone led to longer cortical cell length and LRs in WT in LN, and that the even lower apoplastic pH in *nrt1.1-1* produced even longer cortical cell length and LRs. The longer LRs in *nrt1.1-1* under HN was not correlated with the apoplastic pH. Under LN, the reduced inhibition of AHA2 at S899 in *nrt1.1-1* seems to override the co-occurring slightly decreased phosphorylation at T947, the activating site. Direct interaction of NRT1.1 and AHA2 was not observed by ratiometric bimolecular fluorescence complementation (rBiFC) assays (Figure 2I and S3A), the known interaction of CBL9-CIPK23 and the known absent interaction of CBL9-CIPK14 were used as positive control and negative control, respectively. As NRT1.1 itself cannot phosphorylate AHA2 at different sites, we postulate a kinase exists as a molecular link between NRT1.1 and AHA2 under LN.

Coreceptor QSK1 functions downstream of NRT1.1 to repress LR growth in LN

To assess the potential kinases involved in this NRT1.1-mediated regulation, we ranked phosphorylation sites (based on *p* value) on receptor kinases (Figure 3A and Figure S3B), and found that phosphorylation of the coreceptor QSK1 at S621/S626 was detected in the WT under LN, however, no phosphorylation of QSK1S621/S626 was detectable either in the WT under HN or in *nrt1.1-1* (Figure 3B), while the protein abundance of QSK1 was unchanged (Figure 3C). Therefore, we conclude that NRT1.1 is required for the phosphorylation of QSK1 at S621/S626 under LN. QSK1 phosphorylation at S621/S626 was also found in previous experiments under LN condition.[22,23]

QSK1 is strongly expressed in the root elongation zone and LR primordia[31], which overlaps with the expression pattern of NRT1.1.[12] To investigate whether QSK1 as well as its phosphorylation sites regulates LN-induced LR growth in similar way as NRT1.1, we generated transgenic plants overexpressing QSK1, phospho-dead (AA) and phosphorylation-mimic QSK1 (DD) at S621S626 into *qsk1*. Compared to WT, the LR length was significantly longer in *qsk1* under LN, and QSK1-OE/*qsk1* can complement *qsk1* phenotype. Consistent with the observation of *qsk1* under LN, LR of QSK1-AA-OE/*qsk1* were significantly longer when compared with the WT, while QSK1-DD-OE/*qsk1* displayed the similar phenotype as WT under LN (Figure 3D and 3E), implying that phosphorylation-mimic QSK1 can rescue the phenotype of *qsk1*, repressing LR growth under LN.

Published protein-protein interaction networks from *Arabidopsis* roots suggested that QSK1 may form a complex with NRT1.1 and AHA2 in a LN-dependent manner.[32] rBiFC assays confirmed that NRT1.1 directly interacts with QSK1 in the plasma membrane (Figure 4A and Figure S4A). H356 of NRT1.1 is critical for nitrate binding and uptake.[33,34] To test whether nitrate binding is required for interaction of NRT1.1 with QSK1, we mutated H356 to H356A. Indeed, interaction between NRT1.1H356A and QSK1 was weaker compared to NRT1.1-QSK1 (Figure 4A and Figure S4A). To further test whether LN-induced phosphorylation of NRT1.1 at T101[2] and QSK1 at S621S626 (Figure 3B) are essential for NRT1.1-QSK1 interaction, we analyzed the interaction of different combinations of NRT1.1 and QSK1 mutants. We found that the NRT1.1-QSK1 interaction was not affected by either the phosphorylation-dead (NRT1.1-A) or phosphorylation-mimic version (NRT1.1-D) of NRT1.1T101. The phospho-dead QSK1S621/S626 (QSK1-AA) still interacted with NRT1.1-A, but the interaction of NRT1.1 and QSK1 was significantly enhanced by phosphorylation mimic QSK1 (QSK1-DD) and NRT1.1 (NRT1.1-D) (Figure 4A and Figure S4A). Importantly, co-immunoprecipitation (Co-IP) assays using membrane proteins isolated from tobacco leaves expressing NRT1.1-eGFP and QSK1-FLAG showed that association between NRT1.1-eGFP and QSK1-FLAG was enhanced when LN is present, not HN, suggesting that LN promotes the NRT1.1-QSK1 interaction (Figure 4B). Altogether these results demonstrated that NRT1.1 directly interacts with QSK1, and this interaction is facilitated by the perception of LN by NRT1.1 and subsequent phosphorylation events.

We next created a *nrt1.1-1qsk1* double mutant to analyze the effect on LR growth. Compared to WT, the LRs length was significantly longer in *qsk1*, *nrt1.1-1*, and the *nrt1.1-1qsk1* double mutant in LN, while the LR length in the double mutant resembled that of the two single mutants. At HN, only the *nrt1.1-1* and the *nrt1.1-1qsk1* double mutant showed longer LRs length, with no effect observed in *qsk1* (Figure 4C and 4D). These results suggested that QSK1 and NRT1.1 function in the same signaling pathway to repress LR growth in LN. To elucidate whether QSK1 contributes to nitrate uptake under LN, we performed nitrate influx assays on N starved plant or after induction with 1 mM nitrate for 1 or 4 h (Figure 4E). Nitrate influx was measured after supplying a nutrient solution containing 200μM $K^{15}NO_3$ during 5 minutes. In N starved plants, higher uptake rates were observed in *qsk1* compared to WT. This difference

was not observed when plants were treated with 1 mM NO_3^-. These results indicated that QSK1 inhibits LR growth and nitrate uptake in LN-dependent manner.

QSK1 interacts with and phosphorylates AHA2S899 and represses proton pump activity in LN

To investigate association of QSK1 and AHA2, we then performed rBiFC and Co-IP assays. rBiFC assays confirmed the interaction of QSK1-DD and AHA2, while QSK1-AA and AHA2 interaction was not obvious (Figure 5A and Figure S4B). Using Co-IP assays, a much stronger association was observed between QSK1-DD-FLAG and AHA2-MYC compared to QSK1 or QSK1-AA with AHA2 (Figure 5B).

We next examined the phosphorylation status of AHA2 at T947 and S899 in WT and *qsk1* roots. LN-induced phosphorylation of AHA2 at T947 and S899 was significantly decreased in *qsk1*, while under HN no changes were observed for either phospho-site (Figure 5C and 5D), suggesting that under LN, QSK1 is required for phosphorylation of both sites on AHA2. The protein abundances of AHA2 displayed no change (Figure 5E). The phosphorylation ratio of T947/S899 was also disrupted in *qsk1*, being significantly higher in *qsk1* compared to WT under LN, but not under HN (Figure 5F). The AHA2 phosphorylation patterns found in *qsk1* resemble T947/S899 ratio found in *nrt1.1-1* under LN, implying an increased activity of H^+-ATPase in also *qsk1*. Furthermore, an *in vitro* peptide phosphorylation assay using the recombinant intracellular domain of QSK1 (QSK1C) and synthesized peptides covering S899 or T947 site as substrates, confirmed that QSK1C could phosphorylate S899, but not T947 on the synthesized peptide (Figure 5G).

To verify the role of QSK1 in impeding PM H^+-ATPase activity under LN, we again used HPTS as a pH indicator on the LR elongation zone of WT and *qsk1*. *qsk1* showed lower apoplastic pH in the LR elongation zone under LN compared to WT (Figure 5H and 5I), which correlates with longer cortical cell (Figure 5J and 5K) and LR length (Figure 3E). These results suggested that QSK1 could serve as a downstream component of NRT1.1 and that QSK1 has a key role in repressing apoplast acidification through direct phosphorylation of AHA2 at S899 under LN, not HN condition.

NRT1.1-QSK1 complex coordinately transduce LN sensing to the proton pump

Our results show that LN enhanced NRT1.1-QSK1 interaction (Figure 4B), induced phosphorylation of QSK1 (Figure 3B), and phosphorylated QSK1 displayed stronger association with AHA2 (Figure 5B). Thus, we propose that NRT1.1-mediated LN sensing may modulate the QSK1-AHA2 interaction. To test this hypothesis, we performed Co-IP assays using membrane protein mixture extracted from *Nicotiana benthamiana* leaves harboring NRT1.1-eGFP, QSK1-FLAG and AHA2-MYC in presence of LN, HN, or KCl. A strong interaction between QSK1-FLAG and AHA2-MYC was observed in the presence of LN-NRT1.1, with the interaction becoming weaker in the presence of HN-NRT1.1 or KCl- NRT1.1 (Figure 6A). We also analyzed the effect of LN on apoplast pH and cortical cell length of LRs in double mutant *nrt1.1-1qsk1*. As expected, *nrt1.1-1qsk1* double mutant showed lower apoplastic pH in LR elongation zone and longer cells when compared to WT, but no differences when compared to respective single mutants under LN (Figure 6B and 6C). Together, these results suggested that LN promotes NRT1.1-QSK1-AHA2 complex in order to transduce the LN signal from NRT1.1 to AHA2 through QSK1. Formation of this complex then ultimately results in repression of the proton pump activity through phosphorylation at inhibitory S899, which ultimately then affects cell elongation and nitrate uptake.

Discussion

NRT1.1 is a plasma membrane-localized nitrate transceptor and critical for nitrate binding and sensing. However, it is still poorly understood how NRT1.1 mediates transduction of nitrate signals within plasma membrane localized proteins. Recent findings that NRT1.1 can form a complex with Ca^{2+}channel CNGC15 suggest that protein-protein interactions are the molecular mechanism coupling nitrate sensing and signaling to downstream processes such as Ca^{2+} signaling.[8] Here, based on in-depth membrane phosphoproteomics analysis, our data provide a first unbiased view of NRT1.1-dependent phosphorylation events under LN (Figure 1). A noteworthy finding is that phosphorylation of several receptor kinases and transporters under LN depends on the presence of NRT1.1 (Figure 3A and Figure S1E), for example, three of the known ammonium and nitrate-regulated phosphosites, T460 and S480/S489, in the cytosolic C-terminal region of AtAMT1;1 were identified.[35] This opens the possibility that some of these proteins could be involved in further complexes with NRT1.1 integrating, for example, nitrate and ammonium signaling.

Our work describes a new role of NRT1.1 in modulation of AHA2 activity by formation of a protein-protein interaction complex. This is unlike the ability of NRT1.1 to directly transport auxin.[12,13] Since NRT1.1 is not directly associated with AHA2 (Figure 2I) we postulated that kinases exit between NRT1.1 and AHA2, and at the plasma membrane, receptor kinases are likely candidates linking NRT1.1 and proton pump AHA2 (Figure 3A). Receptor kinases play critical roles in perception and transduction of extracellular signals, as well as in plant growth and defense.[36] Several studies have uncovered that RKs could directly interact with PM-localized transport proteins and regulate their activity. For example, TMK1, PSY1R, and BAK1 are well characterized in activation of AHA2 through phosphorylation modification at different sites on AHA2[27,37-40], while FERONIA can induce phosphorylation of S899 on AHA2, inhibiting proton efflux.[26] FLS2 interacts with Ca^{2+} -ATPase ACA8 to regulate Ca^{2+} bursts[41], and SIRK1 can phosphorylate and activate aquaporins.[42,43] These short, posttranscriptional and direct regulatory circuits between RKs and transport proteins indicates a rapid and economic mechanism, allowing plants to efficiently respond to local signals and rapidly adjust to changes in the environment. Our findings provide a first evidence for a transceptor being linked to another transmembrane transport proteins (here: AHA2) by a receptor kinase, QSK1.

QSK1 (“thousand-hand” qiān shǒu kinase 1) is a highly expressed co-receptor kinase in *Arabidopsis thaliana*. Depending of the physiological state of the plant, it is able to directly phosphorylate specific substrate proteins, such as an ABC camalexin transporter upon fungal infection[44] and potassium channel TPK1 during stomatal closure.[45] It can also recruit substrates such as the aquaporin PIP2;4 to other receptor kinases, such as SIRK1, forming a complex ultimately resulting in substrate phosphorylation.[42,43] Therefore, QSK1 is proposed to be a coreceptor and responsible for recruiting different substrates to the respective signaling complexes. QSK1 is known to be able to change localization, being depleted from ordered low-density membranes (DRM) upon treatment with cytochalasin D or oryzalin.[46] Here, we show that phosphorylated QSK1 recruits and phosphorylates AHA2 under LN (Figure 5).

Posttranslational regulation of PM H^+-ATPases by phosphorylation and dephosphorylation plays a crucial role in the activation or inactivation in response to stress.[47-49] Several phosphorylation sites within the autoinhibitory C-terminal domain of PM H^+-ATPases, which differentially affect pump activity, have been identified.

Among them, phosphorylation at T947 and T881 of AHA2 increases pump activity[27,37,38], while phosphorylation at S899 and S931 inhibits pump activity.[26,50] flg22, a peptide derived from pathogenic bacterial flagella, elicits an increase in phosphorylation at S899 and a decrease at T881 and T947, and leads to a rapid apoplastic alkalinization.[51] PM-localized ATPases regulates H^+ efflux into the apoplast, resulting in apoplastic acidification, which in turn affects LR growth. The proton gradient is also used for ion uptake as well as cell elongation. Also, nitrate uptake has been found to be coupled to protons.[33] We found that the elevated phosphorylation ratio T947/S899 on AHA2 in *nrt1.1-1* and *qsk1* at LN results in higher AHA2 activity and subsequently longer LRs (Figure 2 and Figure 5). Our results show that the PM H^+-ATPase activity is controlled coordinately by the balance of phosphorylation at different sites. Since QSK1 specifically phosphorylates the S899 on AHA2 (Figure 5G), thus, we propose there exist other proteins (e.g., RKs or other Kinases) downstream of NRT1.1 which phosphorylate T947 on AHA2.

It is interesting to note that QSK1 is a coreceptor, not a ligand-binding receptor kinase. Further research will be necessary to identify possible receptor kinase, as well as their ligands, may function in a NRT1.1 dependent or independent manner. As NRT1.1 plays a critical role in the assembly of the here described signaling module, one may speculate that NRT1.1, as a transceptor, functions as a main receptor to transduce the LN signal to co-receptor QSK1. Mild nitrate deficiency activates BR signaling and induces LR elongation[52], while the role of auxin in LN-mediated LR elongation has been well studied.[12,13,53] Additional research will be directed in exploring whether BR and auxin are involved in regulating the NRT1.1-QSK1-AHA2 module.

In summary, we demonstrate that at LN, nitrate binding to NRT1.1 is able to enhance the NRT1.1-QSK1 interaction and phosphorylation of S621S626 on coreceptor QSK1. This is the first example for a nutrient sensing transporter to recruit a co-receptor for signal transduction. Phosphorylated QSK1 then recruits AHA2 into the complex in order to phosphorylate S899 on AHA2. Since also phosphorylation of AHA2 at T947 can be affected by NRT1.1 or QSK1, we suspect further yet unknow kinases to be involved in regulation of AHA2 activity directly or indirectly. (Figure 6D). Our results have not only identified the key role of RKs and proton pump AHA2 under LN signaling but has also coupled LN sensing from NRT1.1 to the activity of the proton pump.

Methods

Plant Material and growth conditions

For liquid growth cultures, *Arabidopsis* seeds of WT (Col-0), *qsk1* mutant (*SALK_019840*), and *nrt1.1-1 mutant* (*SALK_097431*) were sterilized and grown in basal medium composed of micro- and macronutrients with a total of 1 mM KNO_3. After 19 days, seedlings were starved for 2 days by changing the growth medium to a nitrogen-free medium. Nitrate was then resupplied to a final concentration of 0.45 mM (mild low nitrate, LN) and 9.4 mM (high nitrate, HN) for 15 minutes before harvesting roots for microsomal protein preparation. All experiments consisted of at least three biological replicates.

For LR growth analysis, WT (Col-0), *qsk1*, *35S*::QSK1-GFP/*qsk1* (QSK1-OE/ *qsk1*), *35S*::QSK1S621AS626A-GFP/*qsk1* (QSK1-AA-OE/*qsk1*), *35S*::QSK1S621DS626D-GFP/*qsk1* (QSK1-DD-OE/*qsk1*), and *nrt1.1-1* seeds were grown on medium mentioned above with 1% agar and 0.45 mM or 9.4 mM KNO_3 for 10 days in a growth chamber and positioned vertically (16/8 hours light/night). Seedlings were scanned as pictures on the 10^{th} day and LR length was measured using Fiji software.

Constructs

For ratiometric bimolecular fluorescence complementation (rBiFC) of *Arabidopsis* proteins, cDNAs of the following genes were cloned into rBiFC plasmids [54]: NRT1.1, NRT1.1H356A, NRT1.1T101A, NRT1.1T101D and AHA2 were cloned as fusions with the C-terminal half of YFP, whereas QSK1, QSK1 QSK1S621A/S626A, QSK1S621D/S626D were cloned as fusions with the N-terminal half of YFP. All constructs were transformed into *Agrobacterium tumefaciens* strain GV3101 by electroporation. Positive colonies were confirmed by spectinomycin and rifampicin resistance and colony PCR.

For purification of the cytoplasmic domain of QSK1 (QSK1C, amino acid 276–627) were cloned into *Escherichia coli* BL21(DE3) expressing plasmid pETGST1a and fused with His and GST tags, resulting in the plasmid His-GST-SIRK1C and His-GST-QSK1C.

Protein expression and purification

Plasmids His-GST-SIRK1C and His-GST-QSK1C were transformed into *Escherichia coli* BL21 (DE3). After 5 hours induction by IPTG (isopropyl-$_D$-thiogalactopyranoside), cells were harvested and lysed using lysis buffer (20mM Tris-HCl pH 7.4, 1mM EDTA, 200mM NaCl, 1mM PMSF, 1mM DTT), soluble fractions were used over gravity flow Ni^2-NTA Sepharose columns for His-GST-SIRK1C and His-GST-QSK1C protein purification.

Co-immunoprecipitation assays

Membrane protein was extracted from infiltrated Tobacco (*Nicotiana Benthamian*) leaves with IP buffer (50 mM Tris-HCl (pH 7.5), 150 mM NaCl, 1 mM EDTA, 1% Triton X-100, 10% glycerol, 1 mM PMSF, 1× protease inhibitor cocktail), 0.45 mM potassium nitrate or potassium chloride was then added and incubated with anti-GFP magnetic agarose beads (Chromotek, gta-20) for 3 h at 4 °C. The beads were washed five times with wash buffer (50 mM Tris-HCl (pH 7.5), 150 mM NaCl, 1 mM EDTA, 1× protease inhibitor cocktail). The precipitated proteins were eluted with 2×SDS buffer loading buffer at 95 °C for 10 min for immunoblot analysis using the indicated antibodies (Abcam).

Microsomal membrane preparation, tryptic digestion, and phosphopeptide enrichment

Microsomal membrane (MF) preparation and phosphopeptide enrichment were performed as described in the “ShortPhos” workflow [55]. A total of 1 g of roots (fresh weight) was homogenized in 10 ml extraction buffer (330mM sucrose, 100 mM KCl, 1 mM EDTA, 50 mM Tris-MES, fresh 5 mM DTT, and 1 mM phenylmethylsulfonylfluoride, pH 7.5) in the presence of 0.5% v/v proteinase inhibitor mixture (MedChemExpress) and phosphatase inhibitors (25 mM NaF, 1 mM Na_3VO_4, 1 mM benzamidin, 3 µM leupeptin) in Dounce homogenizers. The homogenate was centrifuged for 15 minutes at 7500 × g at 4 °C. The pellet was discarded, and the supernatant was centrifuged for 75 minutes at 48,000 × g at 4 °C. The microsomal pellet was re-suspended in 100 µl UTU (6 M urea, 2 M thiourea, pH 8). Protein concentrations were determined using a Bradford (Sigma–Aldrich) assay with BSA (Bovine serum albumin) as protein standard. Samples were stored at -80°C.

150 µg MF were aliquoted for tryptic digestion and phosphopeptides enrichment. MF were predigested for 3 h with endoproteinase Lys-C (0.5 µg/µl; Wako Chemicals) at

room temperature. After a 4-fold dilution with 10 mM Tris-HCl (pH 8), samples were digested with 3 µl sequencing-grade modified trypsin (0.5 µg/µl; Promega) overnight at 37 °C. After overnight digestion, 10% v/v trifluoroacetic acid (TFA) was added (until the pH was 3 or less) to stop digestion. Digested peptides were dried in a vacuum concentrator.

Dry peptides were dissolved in 200 µl of 1 M glycolic acid in 80% v/v acetonitrile (ACN) and 5% v/v trifluoroacetic acid (TFA). Phosphopeptides were enriched over titanium dioxide (TiO_2) (GL Sciences). 1.5 mg TiO_2 beads per sample were washed once with 100 µl of 1% v/v ammonia solution and equilibrated three times with 50 µl of 1 M glycolic acid in 80% v/v ACN and 6% v/v TFA. 200 µl digested peptides were mixed with equilibrated TiO_2 for 30 min incubation. Peptides and TiO_2 beads mixture were washed once with 100 µl of 1 M glycolic acid in 80% v/v ACN and 6% v/v TFA, and three times with 100 µl of 80% v/v ACN and 1% v/v TFA. Phosphopeptides were eluted from TiO_2 beads three times with 1% v/v ammonia solution. Eluates were immediately acidified with 70 µl of 10% v/v formic acid. Acidified phosphopeptides were desalted over a C18 stage tip prior to mass spectrometric analysis.

LC-MS/MS of Peptides and Phosphopeptides

Enriched phosphopeptides were resuspended in 5 µl resuspension buffer (0.2% v/v TFA, 5% v/v ACN) and analyzed via LC-MS/MS using standard setting as described[33] with nanoflow Easy-nLC 1200 (Thermo Scientific) as an HPLC system and an Orbitrap hybrid mass spectrometer (Orbitrap exploris 480, Thermo Scientific) as a mass analyzer. Peptides were eluted from a 75 µm homemade 25 cm analytical column on a linear gradient running from 4 to 64% acetonitrile over 130 min and sprayed directly into the mass spectrometer. Peptides were identified via MS/MS based on the information-dependent acquisition of fragmentation spectra of multiple charged peptides. A data-dependent acquisition MS method was used, and for full-scan spectrum and MS/MS scan acquired at resolution of 60,000 and 15,000 at m/z 200.

Protein Identification and Ion Intensity Quantitation

Raw data acquired by the mass spectrometer were processed using MaxQuant [56], version 1.6.5.0 using settings as described for protein identification and label-free intensity quantitation (LFQ). Spectra were matched against the *Arabidopsis* proteome UP000006548 (UniProt database, 39,324 entries). Common contaminants (trypsin,

keratin, etc.) were included during database searches. Carbamidomethylation of cysteine was set as a fixed modification, and the oxidized methionine (M), acetylation (protein N-term) and phosphorylation (STY) were set as variable modifications. Trypsin was specified as the digesting protease, and up to two missed cleavages were allowed. The mass tolerance for the database search was set to 20 ppm for full scans and 0.5 Da for ions fragment. The multiplicity was set to 1. For label-free quantitation, retention time matching between runs was chosen within a time window of 0.7 min. False discovery rate cutoffs were set to 0.01 for peptide and protein identification, and to 0.05 for phosphorylation site assignment. Hits to contaminants (e.g., keratins) and reverse hits identified by MaxQuant were excluded from further analysis.

Bioinformatics and statistical Analysis

Bioinformatics analysis was performed with Perseus software (version 1.6.4.0).[57] For the analysis of phosphoproteomic results, reported label free intensity (LFQ) values (Phospho (STY)Sites. txt) were used for data analysis. Missing values were imputed from a normal distribution around the detection limit of the mass spectrometer. For each phosphosite, imputed values from five or six biological replicates in different genotypes or treatment were used for student *t* tests (FDR<0.05, S0=0.1).

Annotations were extracted from MapMan[58], subcellular locations were obtained from SUBA3.[59] Functional enrichment analysis was done via Fisher's exact test, *p* values were adjusted using Bonferroni correction. *p* value indicates a degree of significance and enrichment factor represent the level of enrichment with respect to the background.

Ratiometric bimolecular fluorescence assay

Agrobacterium tumefaciens harboring the relevant constructs described above were injected into 5 to 6 weeks old *Nicotiana benthamiana* leaves for 2 days before observation. Fluorescence was observed using a Zeiss LSM800 confocal microscope (20× water immersion objective). In all cases, excitation intensities, filter settings, photomultiplier gains and other parameters were standardized. The YFP and RFP fluorochromes were excited with 488 nm and 561 nm, respectively. Emitted light was collected at a range of 500–560 nm for YFP and 575–625 nm for RFP. All images throughout all experiments were collected using the same settings. The collected images were processed and both YFP and RFP intensity was measured using the FIJI software and the YFP/RFP ratio was calculated. RFP is internal control. At least 20

different cells from leaves of the 2 plants were analyzed. Statistical significance was determined using one-way ANOVA test with a Tukey test. To calibrate YFP/RFP ratios, known interaction of CBL9 with CIPK23 was used as positive control, whereas the interaction of CBL9 with CIPK14 was used as negative control.[60] YFP/RFP ratio greater than 1 indicate interaction of two proteins, while YFP/RFP ratio smaller than 1 suggest weak or no interaction.

HPTS assay

HPTS staining was performed as described[30] with minor modifications. 10 days old seedlings grown on LN and HN medium were transferred into liquid LN and HN medium supplemented with 1mM HPTS for 30 min. The seedlings were subsequently mounted in the same growth medium supplemented with HPTS on a microcopy slide. HPTS stained images of lateral roots elongation zone was performed using an inverted Zeiss LSM800 confocal microscope equipped with a highly sensitive GaAsP detector. Fluorescent signals for the protonated HPTS form (Excitation 405 nm, emission peak 514 nm), as well as the deprotonated HPTS form (excitation 488 nm, emission peak 514 nm) were detected with a 20× (water immersion) objective. The image analysis was performed using the Fiji macro. The ratiometric value (488/405) correlates with the apoplastic pH. The higher value represents higher pH.

$^{15}NO_3$ influx experiment

Root NO3−influx was assayed as described by Laugier et al.[61] Five weeks old hydroponically-grown plants were nitrate-starved for 5 days, then subjected to 1 mM NO^3 for 0h, 1h or 4h. After washing with 0.1 mM CaSO4, roots were subsequently transferred into a nutrient solution containing 200µM $^{15}NO_3$ (99 atom% excess 15N) for 5 minutes. Roots were harvested and dried at 70°C for 48 h, and samples were analyzed for total N and atom% 15N using a continuous flow isotope ratio mass spectrometer coupled with a C/N elemental analyzer (model Euroflash; Eurovector, Pavia, Italy). 6-12 replicates were performed in each genotype and condition.

An *in vitro* peptide phosphorylation assay

In vitro peptide phosphorylation assays were performed as described in published paper[43] with minor modification. In brief, kinase activity assays were performed with 10 pmol of the peptides GLDIETPSHYTV (covering T947) or EAVNIFPEKGSYR

(covering S899) as a substrate and His-GST-QSK1-Cterminal Domain (QSK1C) as kinases in 30 µl kinase reaction buffer (20 mM Tris/HCl pH 7.5, 10 mM $MgCl_2$, 1 mM $MnCl_2$, 0.1% BSA, 2 mM DTT, 100 µM ATP). After incubation for one hour, the reaction mixture was acidified with TFA. Acidified mixture was then desalted over C18 column. The phosphorylation of peptides was analyzed vis mass spectrometry and quantified based on the intensity of signature fragment ion.

Author contributions

Z.Z and L.K performed most experiments. X.N.W, L.K and W.X.S designed research; S.L ran samples in mass spectrometry; X.L and T.W assisted with confocal microscope for rBiFC; Z.L, Z.H, X.Y and S.G for phosphoproteomic sample preparation; H.L, M.G, M.H and J.Z for partial data analysis. B.N, A.J and L.L for ^{15}N uptake assay. X.N.W, W.X.S and L.K wrote paper.

Data availability

The raw MS data from this study was deposited at the ProteomeXchange Consortium via the PRIDE partner repository with the identifier PXD045818 (User name: reviewer_pxd045818@ebi.ac.uk Password: KiHE8I6e).

Acknowledgments

We thank Prof. Dr. Christopher Grefen (Ruhr-University Bochum, Germany) for the rBiFC plasmids and for detailed instructions for microscopy and image analysis of rBiFC assays.

Funding

Research in our laboratories was supported by the general program of National Natural Science Foundation of China (grant no. 32170272 to X.N.W), Natural Science Foundation of Yunnan province (grant NO. 202301AT070206 to X.N.W), Natural Science Foundation of Yunnan province (grant NO.202101AT070457 to S.L), Natural Science Foundation-Youth of Yunnan province (grant NO. 202101AU070021 to S.L), National Natural Science Foundation of China (grant no. 32070306 to J.Z) and China National Key Program for Research and Development (grant no. 2021YFF1000500 to J.Z).

Declaration of interests

The authors declare no competing interest.

References

1. Zhang, Z., Hu, B., and Chu, C. (2020). Towards understanding the hierarchical nitrogen signalling network in plants. Current opinion in plant biology *55*, 60-65. 10.1016/j.pbi.2020.03.006.
2. Liu, K.H., and Tsay, Y.F. (2003). Switching between the two action modes of the dual-affinity nitrate transporter CHL1 by phosphorylation. EMBO J *22*, 1005-1013. 10.1093/emboj/cdg118.
3. Cerezo, M., Tillard, P., Filleur, S., Munos, S., Daniel-Vedele, F., and Gojon, A. (2001). Major alterations of the regulation of root NO(3)(-) uptake are associated with the mutation of Nrt2.1 and Nrt2.2 genes in Arabidopsis. Plant physiology *127*, 262-271. 10.1104/pp.127.1.262.
4. Wang, W., Hu, B., Li, A., and Chu, C. (2020). NRT1.1s in plants: functions beyond nitrate transport. Journal of experimental botany *71*, 4373-4379. 10.1093/jxb/erz554.
5. Ho, C.H., Lin, S.H., Hu, H.C., and Tsay, Y.F. (2009). CHL1 functions as a nitrate sensor in plants. Cell *138*, 1184-1194. 10.1016/j.cell.2009.07.004.
6. Léran, S., Edel, K.H., Pervent, M., Hashimoto, K., Corratgé-Faillie, C., Offenborn, J.N., Tillard, P., Gojon, A., Kudla, J., and Lacombe, B. (2015). Nitrate sensing and uptake in Arabidopsis are enhanced by ABI2, a phosphatase inactivated by the stress hormone abscisic acid. Science signaling *8*, ra43. 10.1126/scisignal.aaa4829.
7. Riveras, E., Alvarez, J.M., Vidal, E.A., Oses, C., Vega, A., and Gutierrez, R.A. (2015). The Calcium Ion Is a Second Messenger in the Nitrate Signaling Pathway of Arabidopsis. Plant physiology *169*, 1397-1404. 10.1104/pp.15.00961.
8. Wang, X., Feng, C., Tian, L., Hou, C., Tian, W., Hu, B., Zhang, Q., Ren, Z., Niu, Q., Song, J., et al. (2021). A transceptor-channel complex couples nitrate sensing to calcium signaling in Arabidopsis. Mol Plant *14*, 774-786. 10.1016/j.molp.2021.02.005.
9. Liu, K.H., Niu, Y., Konishi, M., Wu, Y., Du, H., Sun Chung, H., Li, L., Boudsocq, M., McCormack, M., Maekawa, S., et al. (2017). Discovery of nitrate-CPK-NLP signalling in central nutrient-growth networks. Nature *545*, 311-316. 10.1038/nature22077.
10. Liu, K.H., Liu, M., Lin, Z., Wang, Z.F., Chen, B., Liu, C., Guo, A., Konishi, M., Yanagisawa, S., Wagner, G., and Sheen, J. (2022). NIN-like protein 7 transcription factor is a plant nitrate sensor. Science *377*, 1419-1425. 10.1126/science.add1104.
11. Hu, B., Jiang, Z., Wang, W., Qiu, Y., Zhang, Z., Liu, Y., Li, A., Gao, X., Liu, L., Qian, Y., et al. (2019). Nitrate-NRT1.1B-SPX4 cascade integrates nitrogen and phosphorus signalling networks in plants. Nat Plants *5*, 401-413. 10.1038/s41477-019-0384-1.

12. Bouguyon, E., Brun, F., Meynard, D., Kubes, M., Pervent, M., Leran, S., Lacombe, B., Krouk, G., Guiderdoni, E., Zazimalova, E., et al. (2015). Multiple mechanisms of nitrate sensing by Arabidopsis nitrate transceptor NRT1.1. Nat Plants *1*, 15015. 10.1038/nplants.2015.15.
13. Krouk, G., Lacombe, B., Bielach, A., Perrine-Walker, F., Malinska, K., Mounier, E., Hoyerova, K., Tillard, P., Leon, S., Ljung, K., et al. (2010). Nitrate-regulated auxin transport by NRT1.1 defines a mechanism for nutrient sensing in plants. Dev Cell *18*, 927-937. 10.1016/j.devcel.2010.05.008.
14. Maghiaoui, A., Bouguyon, E., Cuesta, C., Perrine-Walker, F., Alcon, C., Krouk, G., Benkova, E., Nacry, P., Gojon, A., and Bach, L. (2020). The Arabidopsis NRT1.1 transceptor coordinately controls auxin biosynthesis and transport to regulate root branching in response to nitrate. Journal of experimental botany *71*, 4480-4494. 10.1093/jxb/eraa242.
15. Hager, A., Frenzel, R., and Laible, D. (1980). ATP-dependent proton transport into vesicles of microsomal membranes of Zea mays coleoptiles. Zeitschrift fur Naturforschung. Section C, Biosciences *35*, 783-793. 10.1515/znc-1980-9-1021.
16. Wright, L.Z., and Rayle, D.L. (1983). Evidence for a Relationship between H Excretion and Auxin in Shoot Gravitropism. Plant physiology *72*, 99-104. 10.1104/pp.72.1.99.
17. Glass, A.D., Britto, D.T., Kaiser, B.N., Kinghorn, J.R., Kronzucker, H.J., Kumar, A., Okamoto, M., Rawat, S., Siddiqi, M.Y., Unkles, S.E., and Vidmar, J.J. (2002). The regulation of nitrate and ammonium transport systems in plants. Journal of experimental botany *53*, 855-864. 10.1093/jexbot/53.370.855.
18. Lejay, L., Tillard, P., Lepetit, M., Olive, F., Filleur, S., Daniel-Vedele, F., and Gojon, A. (1999). Molecular and functional regulation of two NO3- uptake systems by N- and C-status of Arabidopsis plants. The Plant journal : for cell and molecular biology *18*, 509-519. 10.1046/j.1365-313x.1999.00480.x.
19. Scheible, W.R., Morcuende, R., Czechowski, T., Fritz, C., Osuna, D., Palacios-Rojas, N., Schindelasch, D., Thimm, O., Udvardi, M.K., and Stitt, M. (2004). Genome-wide reprogramming of primary and secondary metabolism, protein synthesis, cellular growth processes, and the regulatory infrastructure of Arabidopsis in response to nitrogen. Plant physiology *136*, 2483-2499. 10.1104/pp.104.047019.
20. Jacquot, A., Li, Z., Gojon, A., Schulze, W., and Lejay, L. (2017). Post-translational regulation of nitrogen transporters in plants and microorganisms. Journal of experimental botany *68*, 2567-2580. 10.1093/jxb/erx073.
21. Chu, L.C., Offenborn, J.N., Steinhorst, L., Wu, X.N., Xi, L., Li, Z., Jacquot, A., Lejay, L., Kudla, J., and Schulze, W.X. (2021). Plasma membrane calcineurin B-like calcium-ion sensor proteins function in regulating primary root growth and nitrate uptake by

affecting global phosphorylation patterns and microdomain protein distribution. New Phytol *229*, 2223-2237. 10.1111/nph.17017.

22. ngelsberger, W.R., and Schulze, W.X. (2012). Nitrate and ammonium lead to distinct global dynamic phosphorylation patterns when resupplied to nitrogen starved Arabidopsis seedlings. The Plant Journal *69*, 978-995.

23. Menz, J., Li, Z., Schulze, W.X., and Ludewig, U. (2016). Early nitrogen-deprivation responses in Arabidopsis roots reveal distinct differences on transcriptome and (phospho-) proteome levels between nitrate and ammonium nutrition. The Plant journal : for cell and molecular biology *88*, 717-734. 10.1111/tpj.13272.

24. Vega, A., Fredes, I., O'Brien, J., Shen, Z., Otvos, K., Abualia, R., Benkova, E., Briggs, S.P., and Gutierrez, R.A. (2021). Nitrate triggered phosphoproteome changes and a PIN2 phosphosite modulating root system architecture. EMBO Rep *22*, e51813. 10.15252/embr.202051813.

25. Durek, P., Schmidt, R., Heazlewood, J.L., Jones, A., MacLean, D., Nagel, A., Kersten, B., and Schulze, W.X. (2010). PhosPhAt: The Arabidopsis thaliana phosphorylation site database. An update. Nucleic Acids Research *38*, D828-D834.

26. Haruta, M., Sabat, G., Stecker, K., Minkoff, B.B., and Sussman, M.R. (2014). A peptide hormone and its receptor protein kinase regulates plant cell expansion. Science *343*, 408-411.

27. Lin, W., Zhou, X., Tang, W., Takahashi, K., Pan, X., Dai, J., Ren, H., Zhu, X., Pan, S., Zheng, H., et al. (2021). TMK-based cell-surface auxin signalling activates cell-wall acidification. Nature *599*, 278-282. 10.1038/s41586-021-03976-4.

28. Pedersen, B.P., Buch-Pedersen, M.J., Morth, J.P., Palmgren, M.G., and Nissen, P. (2007). Crystal structure of the plasma membrane proton pump. Nature *450*, 1111-1114. 10.1038/nature06417.

29. Mlodzinska, E., Klobus, G., Christensen, M.D., and Fuglsang, A.T. (2015). The plasma membrane H(+) -ATPase AHA2 contributes to the root architecture in response to different nitrogen supply. Physiol Plant *154*, 270-282. 10.1111/ppl.12305.

30. Barbez, E., Dunser, K., Gaidora, A., Lendl, T., and Busch, W. (2017). Auxin steers root cell expansion via apoplastic pH regulation in Arabidopsis thaliana. Proc Natl Acad Sci U S A *114*, E4884-E4893. 10.1073/pnas.1613499114.

31. Wu, Y., Xun, Q., Guo, Y., Zhang, J., Cheng, K., Shi, T., He, K., Hou, S., Gou, X., and Li, J. (2016). Genome-Wide Expression Pattern Analyses of the Arabidopsis Leucine-Rich Repeat Receptor-Like Kinases. Mol Plant *9*, 289-300. 10.1016/j.molp.2015.12.011.

32. Gilbert, M., Li, Z., Wu, X.N., Rohr, L., Gombos, S., Harter, K., and Schulze, W.X. (2021). Comparison of path-based centrality measures in protein-protein interaction networks revealed proteins with phenotypic relevance during adaptation to changing nitrogen environments. J Proteomics *235*, 104114. 10.1016/j.jprot.2021.104114.

33. Parker, J.L., and Newstead, S. (2014). Molecular basis of nitrate uptake by the plant nitrate transporter NRT1.1. Nature *507*, 68-72. 10.1038/nature13116.
34. Sun, J., Bankston, J.R., Payandeh, J., Hinds, T.R., Zagotta, W.N., and Zheng, N. (2014). Crystal structure of the plant dual-affinity nitrate transporter NRT1.1. Nature *507*, 73-77. 10.1038/nature13074.
35. Wu, X., Liu, T., Zhang, Y., Duan, F., Neuhauser, B., Ludewig, U., Schulze, W.X., and Yuan, L. (2019). Ammonium and nitrate regulate NH4+ uptake activity of Arabidopsis ammonium transporter AtAMT1;3 via phosphorylation at multiple C-terminal sites. Journal of experimental botany *70*, 4919-4930. 10.1093/jxb/erz230.
36. Shiu, S.-H., and Bleecker, A.B. (2001). Receptor-like kinases form *Arabidopsis* form a monophyletic gene family related to animal receptor kinases. Proceedings of the National Academy of Sciences of the USA *98*, 10763-10768.
37. Fuglsang, A.T., Kristensen, A., Cuin, T.A., Schulze, W.X., Persson, J., Thuesen, K.H., Ytting, C.K., Oehlenschlaeger, C.B., Mahmood, K., Sondergaard, T.E., et al. (2014). Receptor kinase-mediated control of primary active proton pumping at the plasma membrane. The Plant journal : for cell and molecular biology *80*, 951-964. 10.1111/tpj.12680.
38. Li, L., Verstraeten, I., Roosjen, M., Takahashi, K., Rodriguez, L., Merrin, J., Chen, J., Shabala, L., Smet, W., Ren, H., et al. (2021). Cell surface and intracellular auxin signalling for H(+) fluxes in root growth. Nature *599*, 273-277. 10.1038/s41586-021-04037-6.
39. Pei, D., Hua, D., Deng, J., Wang, Z., Song, C., Wang, Y., Wang, Y., Qi, J., Kollist, H., Yang, S., et al. (2022). Phosphorylation of the plasma membrane H+-ATPase AHA2 by BAK1 is required for ABA-induced stomatal closure in Arabidopsis. Plant Cell *34*, 2708-2729. 10.1093/plcell/koac106.
40. Wang, Z.F., Xie, Z.M., Tan, Y.L., Li, J.Y., Wang, F.L., Pei, D., Li, Z., Guo, Y., Gong, Z., and Wang, Y. (2022). Receptor-like protein kinase BAK1 promotes K+ uptake by regulating H+-ATPase AHA2 under low potassium stress. Plant physiology *189*, 2227-2243. 10.1093/plphys/kiac237.
41. Frei dit Frey, N., Mbengue, M., Kwaaitaal, M., Nitsch, L., Altenbach, D., Haweker, H., Lozano-Duran, R., Njo, M.F., Beeckman, T., Huettel, B., et al. (2012). Plasma membrane calcium ATPases are important components of receptor-mediated signaling in plant immune responses and development. Plant physiology *159*, 798-809. 10.1104/pp.111.192575.
42. Wang, J., Xi, L., Wu, X.N., Konig, S., Rohr, L., Neumann, T., Weber, J., Harter, K., and Schulze, W.X. (2022). PEP7 acts as a peptide ligand for the receptor kinase SIRK1 to regulate aquaporin-mediated water influx and lateral root growth. Mol Plant *15*, 1615-1631. 10.1016/j.molp.2022.09.016.

43. Wu, X.N., Chu, L., Xi, L., Pertl-Obermeyer, H., Li, Z., Sklodowski, K., Sanchez-Rodriguez, C., Obermeyer, G., and Schulze, W.X. (2019). Sucrose-induced Receptor Kinase 1 is Modulated by an Interacting Kinase with Short Extracellular Domain. Molecular & cellular proteomics : MCP *18*, 1556-1571. 10.1074/mcp.RA119.001336.
44. Aryal, B., Xia, J., Hu, Z., Stumpe, M., Tsering, T., Liu, J., Huynh, J., Fukao, Y., Glöckner, N., Huang, H.Y., et al. (2023). An LRR receptor kinase controls ABC transporter substrate preferences during plant growth-defense decisions. Current biology : CB *33*, 2008-2023.e2008. 10.1016/j.cub.2023.04.029.
45. Isner, J.C., Begum, A., Nuehse, T., Hetherington, A.M., and Maathuis, F.J.M. (2018). KIN7 Kinase Regulates the Vacuolar TPK1 K(+) Channel during Stomatal Closure. Current biology : CB *28*, 466-472.e464. 10.1016/j.cub.2017.12.046.
46. Szymanski, W.G., Zauber, H., Erban, A., Gorka, M., Wu, X.N., and Schulze, W.X. (2015). Cytoskeletal Components Define Protein Location to Membrane Microdomains. Molecular & cellular proteomics : MCP *14*, 2493-2509. 10.1074/mcp.M114.046904.
47. Bjork, P.K., Rasmussen, S.A., Gjetting, S.K., Havshoi, N.W., Petersen, T.I., Ipsen, J.O., Larsen, T.O., and Fuglsang, A.T. (2020). Tenuazonic acid from Stemphylium loti inhibits the plant plasma membrane H(+) -ATPase by a mechanism involving the C-terminal regulatory domain. New Phytol *226*, 770-784. 10.1111/nph.16398.
48. Miao, R., Yuan, W., Wang, Y., Garcia-Maquilon, I., Dang, X., Li, Y., Zhang, J., Zhu, Y., Rodriguez, P.L., and Xu, W. (2021). Low ABA concentration promotes root growth and hydrotropism through relief of ABA INSENSITIVE 1-mediated inhibition of plasma membrane H(+)-ATPase 2. Science advances *7*. 10.1126/sciadv.abd4113.
49. Rudashevskaya, E.L., Ye, J., Jensen, O.N., Fuglsang, A.T., and Palmgren, M.G. (2012). Phosphosite mapping of P-type plasma membrane H+-ATPase in homologous and heterologous environments. J Biol Chem *287*, 4904-4913. 10.1074/jbc.M111.307264.
50. Fuglsang, A.T., Guo, Y., Cuin, T.A., Qiu, Q., Song, C., Kristiansen, K.A., Bych, K., Schulz, A., Shabala, S., Schumaker, K.S., et al. (2007). Arabidopsis protein kinase PKS5 inhibits the plasma membrane H+ -ATPase by preventing interaction with 14-3-3 protein. Plant Cell *19*, 1617-1634. 10.1105/tpc.105.035626.
51. Nühse, T.S., Bottrill, A.R., Jones, A.M., and Peck, S.C. (2007). Quantitative phosphoproteomic analysis of plasma membrane proteins reveals regulatory mechanisms of plant innate immune responses. The Plant journal : for cell and molecular biology *51*, 931-940. 10.1111/j.1365-313X.2007.03192.x.

52. Jia, Z., Giehl, R.F.H., Meyer, R.C., Altmann, T., and von Wiren, N. (2019). Natural variation of BSK3 tunes brassinosteroid signaling to regulate root foraging under low nitrogen. Nat Commun *10*, 2378. 10.1038/s41467-019-10331-9.
53. Jia, Z., Giehl, R.F.H., and von Wiren, N. (2021). Local auxin biosynthesis acts downstream of brassinosteroids to trigger root foraging for nitrogen. Nat Commun *12*, 5437. 10.1038/s41467-021-25250-x.
54. Grefen, C., and Blatt, M.R. (2012). A 2in1 cloning system enables ratiometric bimolecular fluorescence complementation (rBiFC). Biotechniques *53*, 311-314. 10.2144/000113941.
55. Wu, X.N., Xi, L., Pertl-Obermeyer, H., Li, Z., Chu, L.C., and Schulze, W.X. (2017). Highly Efficient Single-Step Enrichment of Low Abundance Phosphopeptides from Plant Membrane Preparations. Front Plant Sci *8*, 1673. 10.3389/fpls.2017.01673.
56. Cox, J., and Mann, M. (2008). MaxQuant enables high peptide identification rates, individualized p.p.b.-range mass accuracies and proteome-wide protein quantification. Nat Biotechnol *26*, 1367-1372. 10.1038/nbt.1511.
57. Tyanova, S., Temu, T., Sinitcyn, P., Carlson, A., Hein, M.Y., Geiger, T., Mann, M., and Cox, J. (2016). The Perseus computational platform for comprehensive analysis of (prote)omics data. Nat Methods *13*, 731-740. 10.1038/nmeth.3901.
58. Thimm, O., Bläsing, O., Gibon, Y., Nagel, A., Meyer, S., Kruger, P., Selbig, J., Muller, L.A., Rhee, S.Y., and Stitt, M. (2004). MAPMAN: a user-driven tool to display genomics data sets onto diagrams of metabolic pathways and other biological processes. The Plant Journal *37*, 914-939.
59. Tanz, S.K., Castleden, I., Hooper, C.M., Vacher, M., Small, I., and Millar, H.A. (2013). SUBA3: a database for integrating experimentation and prediction to define the SUBcellular location of proteins in Arabidopsis. Nucleic Acids Research *41*, D1185-1191.
60. Cheong, Y.H., Pandey, G.K., Grant, J.J., Batistic, O., Li, L., Kim, B.G., Lee, S.C., Kudla, J., and Luan, S. (2007). Two calcineurin B-like calcium sensors, interacting with protein kinase CIPK23, regulate leaf transpiration and root potassium uptake in Arabidopsis. The Plant journal : for cell and molecular biology *52*, 223-239. 10.1111/j.1365-313X.2007.03236.x.
61. Laugier, E., Bouguyon, E., Mauries, A., Tillard, P., Gojon, A., and Lejay, L. (2012). Regulation of high-affinity nitrate uptake in roots of Arabidopsis depends predominantly on posttranscriptional control of the NRT2.1/NAR2.1 transport system. Plant physiology *158*, 1067-1078. 10.1104/pp.111.188532.

Figure legends

Figure 1. The global membrane phosphoproteome of Arabidopsis roots was changed in the *nrt1.1-1* mutant under LN condition

(A) The work flow of High-throughput phosphoproteomics to identify NRT1.1-mediated LN and HN-induced signaling components.
(B) Principal components analysis (PCA) of WT and *nrt1.1-1* under LN and HN conditions. The first and second components are shown.
(C) Student *t*-test difference between LN-induced and nitrogen starvation (NS) at membrane phosphoproteome (*x* axis) and the difference between HN-induced and nitrogen starvation (NS) in membrane phosphoproteome (*y* axis) in WT. Significant phosphosites were determined using a permutation-based false discovery rate calculation (FDR ≤ 0.05, S0 = 0.1). The phosphosites were colored for significant changed abundance in x axis (orange), y axis (red), and both (purple), respectively.
(D) Student *t*-test difference between *nrt1.1-1* and WT in LN-induced membrane phosphoproteome (*x* axis) and the difference between *nrt1.1-1* and WT in HN-induced membrane phosphoproteome (*y* axis). Significant phosphosites were determined using a permutation-based false discovery rate calculation (FDR ≤ 0.05, S0 = 0.1). The phosphosites were colored for significant changed abundance in x axis (green), y axis (blue) and, both (black), respectively.
(E) Venn diagram showing overlap for phosphosites with significantly changed phosphorylation under LN compared to HN (C) and *nrt1.1-1* compared to WT in LN (D).
(F) Fisher exact test (2% FDR) on the group of 307 phosphosites corresponding to 231 proteins that are indicated in (E). Enriched Mapman terms and SUBA are displayed.

Figure 2. NRT1.1 represses T947/S899 phosphorylation ratio on AHA2 and proton pump activity in LN

(A and B) Difference of phosphorylation levels induced by LN and HN at T947 and S899 sites of PM H+-ATPase AHA2 in WT and nrt1.1-1.
(C) Difference in protein levels of AHA2 induced by LN and HN in WT and nrt1.1-1.
(D) Box plots show T947/S899 phosphorylation ratio for WT and nrt1.1-1 under LN and HN. Center lines of boxes represent medians, vertical line indicate the minimal/maximal value.
Data are mean + SD, at least 4 biological replicates (A-D), statistical analysis (A-D) was performed using Student t-test (****P<0.0001; NS, not significant).
(E and F) Quantification (E) and confocal images (F) of apoplastic pH in the lateral root elongation zone (EZ) of WT and nrt1.1-1 grown in LN and HN medium. Ratiometric value (488 nm/405 nm) of fluorescent HPST was used to monitor pH in the EZ of lateral roots, n≥38 individual root for each. For F, scale bar, 20 μm.
(G and H) Quantification (G) and images (H) of cortical cell length of lateral roots mature zone of WT and *nrt1.1-1* grown in LN and HN medium, n≥63 cells for each. For H, scale bar, 50 μm. Statistical analysis (E and G) was performed using one-way ANOVA with a Tukey test (****P<0.0001; NS, not significant).
(I) Quantification of the in vivo interaction of NRT1.1, with AHA2. Around 20 randomly selected cells were quantified. The known interaction of CBL9-CIPK23 and the known absent interaction of CBL9-CIPK14 were used as positive control and negative control, respectively. Scale bar, 20 μm. Different letters represent significant differences at p<0.05 according to one-way ANOVA with a Tukey test.

Figure 3. LN promotes NRT1.1-QSK1 interaction and QSK1 phosphorylation

(A) Ranking of phosphosites significantly upregulated in WT under LN and downregulated in *nrt1.1-1* in LN. 10 named receptor-like kinases are highlighted in red.
(B) Phosphorylation differences of S621/S626 on QSK1 in WT and *nrt1.1-1* induced by LN and HN.
(C) Differences of protein levels in QSK1 induced by LN and HN in WT and *nrt1.1-1*.
Data are mean + SD, at least 4 biological replicates (B-C), statistical analysis (B-C) was performed using Student *t*-test (different letter indicates P<0.05).
(D) Representative images of WT, *qsk1,* transgenic line overexpressing QSK1, QSK1 phospho-dead and as well as phosphorylation-mimic version in *qsk1* mutant (QSK1-OE/*qsk1,* QSK1-AA-OE/*qsk1* and QSK1-DD-OE/*qsk1*) in LN and HN medium, scale bar 1cm.
(E) Total lateral root length of WT, *qsk1*, QSK1-OE/*qsk1,* QSK1-AA-OE/*qsk1* and QSK1-DD-OE/*qsk1* in LN and HN medium. Bar plots indicate means ± SEM (at least 17 independent seedlings). Lateral roots were measured after 8 days on LN and HN. Statistical analysiswas performed using one-way ANOVA (****P<0.0001; NS, not significant).

Figure 4. QSK1 functions downstream of NRT1.1 to modulate LRs growth in LN

(A) Quantification of the *in vivo* rBiFC interaction of QSK1, QSK1SASA, and QSK1SDSD with NRT1.1, NRT1.1H356A, NRT1.1T01A, and NRT1.1T01D. rBiFC calibration is shown in Figure S3. 18-35 randomly selected cells were quantified.
(B) Co-IP assays using membrane protein mixture extracted from tobacco leaves (*Nicotiana benthamiana*) expressing NRT1.1-eGFP and QSK1-FLAG in the presence of LN (0.45 mM KNO_3), HN (9.4 mM KNO_3) or potassium chloride (0.45 mM).
(C) Representative images of WT, *nrt1.1-1*, *qsk1* and *nrt1.1-1qsk1* in LN and HN medium, scale bar, 1cm. Different letters (A and D) represent significant differences at $p<0.05$ according to one-way ANOVA with a Tukey test.
(D) Total lateral root length of WT, *nrt1.1-1*, *qsk1*, and *nrt1.1-1qsk1* in LN and HN medium. Bar plots indicate means ± SEM (16-20 independent seedlings). Lateral roots were measured after 10 days on LN and HN medium.
Different letters (A and D) represent significant differences at $p<0.05$ according to one-way ANOVA with a Tukey test.
(E) ^{15}Nitrate uptake activity under LN. Bar plots indicate means ± SEM (at least 10 biological replicates). Statistical analysis was performed using two-tailed Student *t*-test ($P<0.05$; NS, not significant).

Figure 5. phosphorylated QSK1 forms a strong complex with AHA2 and represses proton pump activity in LN

(A) Quantification of the *in vivo* rBiFC interaction of QSK1, QSK1SASA and QSK1SDSD with AHA2. rBiFC calibration is shown in Figure S3. 50 randomly selected cells were quantified. Different letters represent significant differences at $p<0.05$ according to one-way ANOVA with a Tukey test.
(B) Co-IP assays using membrane protein mixture extracted from tobacco leaves (*Nicotiana benthamiana*) expressing QSK1-FLAG, QSK1-AA-FLAG and QSK1-DD-FLAG with AHA2-MYC.
(C and D) Difference of phosphorylation levels of T947 (C) and S899 (D) on AHA2 induced by LN and HN in WT and *qsk1*.
(E) Difference of protein levels of AHA2 under LN and HN in WT and *qsk1*.
(F) Box plots show T947/S899 phosphorylation ratio for WT and *qsk1* under LN. Center lines of boxes represent medians, vertical line indicates the minimal/maximal value.
Data (C, D and E) are mean+SD. Statistical analysis (C-F) was performed using two-tailed Student *t*-test (****$P<0.0001$; NS, not significant).
(G) *In vitro* peptide phosphorylation assay using GLDIETPSHY**T**V (covering T947) and EAVNIFPEKG**S**YR (covering S899) from AHA2 as substrates for the QSK1C terminus. nd indicates not detected.
(H and I) Quantification (H) and confocal images (I) of apoplastic pH in the lateral root EZ of WT and *qsk1* grown on LN and HN medium. Ratiometric value (488 nm/405 nm)

of fluorescent HPST was used to monitor pH in the EZ of lateral roots, n≥39 individual root for each. For I, scale bar 20 μm.
(J and K) Quantification (J) and images (K) of cortical cell length of the lateral roots mature zone of WT and *qsk1* grown on LN and HN medium. n≥61 cells for each. For K, scale bar 50 μm.
Statistical analysis (H and J) was performed using one-way ANOVA with a Tukey test (****P<0.0001; NS, not significant).

Figure 6. NRT1.1-QSK1 complex regulates AHA2 activity in LN

(A) Co-IP assays using membrane protein mixture extracted from tobacco leaves (*Nicotiana benthamiana*) expressing NRT1.1-eGFP, QSK1-FLAG and AHA2 in the presence of LN (0.45 mM KNO_3), HN (9.4 mM KNO_3) or potassium chloride (0.45 mM).
(B) Quantification of apoplastic pH in the lateral root EZ of WT, *nrt1.1-1*, *qsk1* and *nrt1.1-1qsk1* grown in LN and HN medium. Ratiometric value (488 nm/405 nm) of fluorescent HPST was used to monitor pH in the EZ of lateral roots, n≥16 individual root for each.
(C) Quantification of the cortical cell length of lateral roots mature zone of WT, *nrt1.1-1*, *qsk1* and *nrt1.1-1qsk1* grown on LN and HN medium, n≥152 cells for each.
Statistical analysis (B and C) was performed using one-way ANOVA with a Tukey test (****P<0.0001; NS, not significant).
(D) Proposed model for LN signal transduction through NRT1.1-QSK1 to AHA2. Perception of LN leads to NRT1.1 interacting with and phosphorylation of QSK1. Subsequently QSK1 recruits AHA2 and directly phosphorylates AHA2S899. NRT1.1 and QSK1 also induces AHA2T947 phosphorylation indirectly through unknown proteins (e.g. Kinases). As a result, phosphorylation ratio of T947/S899 and thus H+-ATPase activity is affected. In both the *nrt1.1-1* and *qsk1* mutants, phosphorylation ratio of T947/S899 is dramatically increased due to a stronger reduction of phosphorylation at S899, resulting in an even higher proton activity, longer cells and longer LRs.

Supplementary Figures and Tables

Figure S1 The global phosphoproteome of *Arabidopsis* roots of WT and *nrt1.1-1* under LN and HN-induced conditions.

(A) Distribution of the assigned phosphorylated amino acid residues for class I phosphosites.
(B) Venn diagram showing the overlap of the phosphosites identified in this study and published in previous nitrate-induced experiments.
(C) Venn diagram showing the overlap of the phosphosites identified in this study and published in previous nitrate-induced experiments.
(D) Summary of identified and quantified class I phosphosites (localization probability of >0.75) corresponding to number of proteins in this study.

(E) Ranking of phosphosites significantly upregulated in WT under LN and downregulated in *nrt1.1-1* in LN. 19 named transport proteins are highlighted in blue.

Figure S2 (A and B) Representative spectra of AHA2 C-terminal peptides GLDIETPSHYTV (containing phosphorylated T947 (A) and EAVNIFPEKGSYR (containing phosphorylated S899) (B) directly exported from MaxQuant version 1.6.4.0. The phosphorylated amino acid is indicated by (ph).

(C) Representative images for total lateral root length of WT and *nrt1.1-1* in LN and HN, scale bar 1cm.

(D) Total lateral root length of WT and *nrt1.1-1* in LN and HN. Bar plots indicate means ± SEM (at least 16 independent seedlings). Lateral roots were measured after 10 days on LN and HN medium. Different letters represent significant differences at $P<0.05$ according to one-way ANOVA.

Figure S3 (A) Representative images of the in vivo interaction of NRT1.1, with AHA2. The known interaction of CBL9-CIPK23 and the known absent interaction of CBL9-CIPK14 were used as positive control and negative control, respectively. Cartoons show the respective T-DNA of the rBiFC-2in1-CC vector, harboring different versions of CIPK23-nYFP and CIPK14-nYFP with cYFP-CBL9, NRT1.1-cYFP and AHA2-nYFP. Scale bar, 20µm.

(B) Representative spectra of QSK1 C-terminal peptides LIEEVSHSSGSPNPVSD (containing phosphorylated S621S626) directly exported from MaxQuant version 1.6.4.0. The phosphorylated amino acid is indicated by (ph).

Figure S4 (A) Representative images of the in vivo interaction of QSK1, QSK1SASA, and QSK1SDSD with NRT1.1, NRT1.1H356A, NRT1.1T01A, and NRT1.1T01D.

(B) Representative images of the in vivo interaction of QSK1, QSK1SASA and QSK1SDSD with AHA2 (C).

Cartoons show the respective T-DNA of the rBiFC-2in1-CC vector, harboring different versions of QSK1s-nYFP, NRT1.1s-cYFP and AHA2-cYFP. Scale bar, 20µm.

Supplementary Table 1 Quantitative phospho-profiling in WT and *nrt1.1-1* mutant.

Figures:

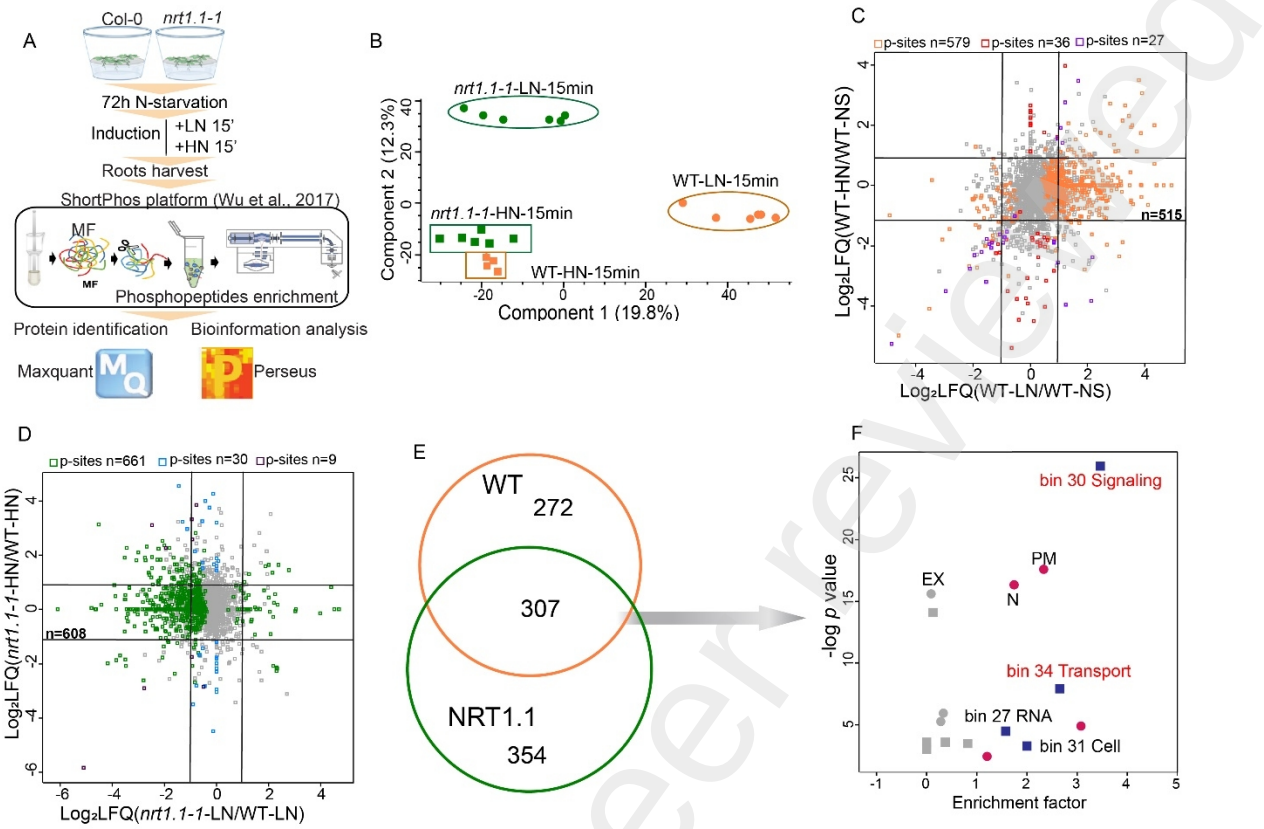

Figure 1. The global membrane phosphoproteome of *Arabidopsis* roots was changed in the *nrt1.1-1* mutant under LN condition

(A) The work flow of High-throughput phosphoproteomics to identify NRT1.1-mediated LN and HN-induced signaling components.

(B) Principal components analysis (PCA) of WT and *nrt1.1-1* under LN and HN conditions. The first and second components are shown.

(C) Student *t*-test difference between LN-induced and nitrogen starvation (NS) at membrane phosphoproteome (*x* axis) and the difference between HN-induced and nitrogen starvation (NS) in membrane phosphoproteome (*y* axis) in WT. Significant phosphosites were determined using a permutation-based false discovery rate calculation (FDR ≤ 0.05, S0 = 0.1). The phosphosites were colored for significant changed abundance in x axis (orange), y axis (red), and both (purple), respectively.

(D) Student *t*-test difference between *nrt1.1-1* and WT in LN-induced membrane phosphoproteome (*x* axis) and the difference between *nrt1.1-1* and WT in HN-induced membrane phosphoproteome (*y* axis). Significant phosphosites were determined using a permutation-based false discovery rate calculation (FDR ≤ 0.05, S0 = 0.1). The phosphosites were colored for significant changed abundance in x axis (green), y axis (blue) and, both (black), respectively.

(E) Venn diagram showing overlap for phosphosites with significantly changed phosphorylation under LN compared to HN (C) and *nrt1.1-1* compared to WT in LN (D).

(F) Fisher exact test (2% FDR) on the group of 307 phosphosites corresponding to 231 proteins that are indicated in (E). Enriched Mapman terms and SUBA are displayed.

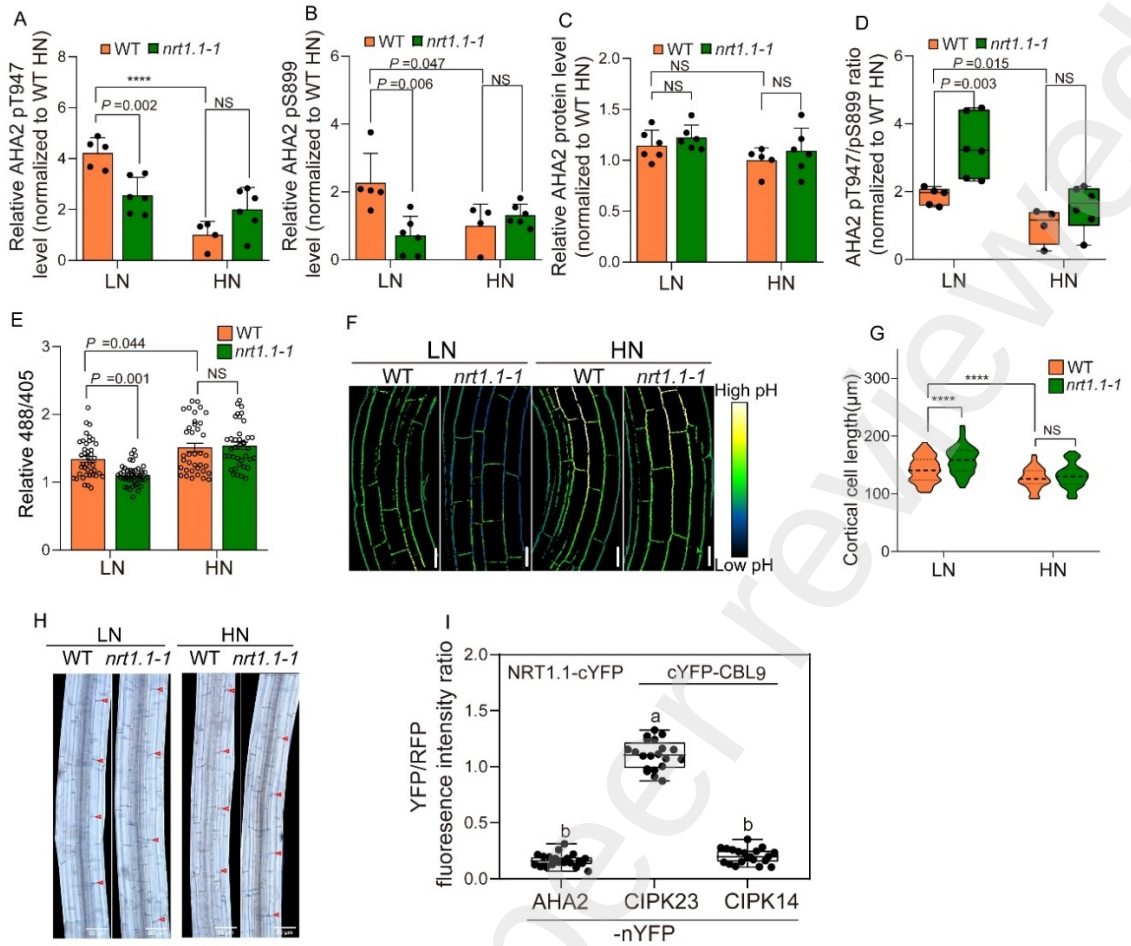

Figure 2. NRT1.1 represses T947/S899 phosphorylation ratio on AHA2 and proton pump activity in LN

(A and B) Difference of phosphorylation levels induced by LN and HN at T947 and S899 sites of PM H^+-ATPase AHA2 in WT and *nrt1.1-1*.

(C) Difference in protein levels of AHA2 induced by LN and HN in WT and *nrt1.1-1*.

(D) Box plots show T947/S899 phosphorylation ratio for WT and *nrt1.1-1* under LN and HN. Center lines of boxes represent medians, vertical line indicate the minimal/maximal value.

Data are mean + SD, at least 4 biological replicates (A-D), statistical analysis (A-D) was performed using Student *t*-test (****P<0.0001; NS, not significant).

(E and F) Quantification (E) and confocal images (F) of apoplastic pH in the lateral root elongation zone (EZ) of WT and *nrt1.1-1* grown in LN and HN medium. Ratiometric value (488 nm/405 nm) of fluorescent HPST was used to monitor pH in the EZ of lateral roots, $n \geq 38$ individual root for each. For F, scale bar, 20 μm.

(G and H) Quantification (G) and images (H) of cortical cell length of lateral roots mature zone of WT and *nrt1.1-1* grown in LN and HN medium, $n \geq 63$ cells for each. For H, scale bar, 50 μm. Statistical analysis (E and G) was performed using one-way ANOVA with a Tukey test (****P<0.0001; NS, not significant).

(I) Quantification of the *in vivo* interaction of NRT1.1, with AHA2. Around 20 randomly selected cells were quantified. The known interaction of CBL9-CIPK23 and the known absent interaction of CBL9-CIPK14 were used as positive control and negative control, respectively. Different

letters represent significant differences at $p<0.05$ according to one-way ANOVA with a Tukey test.

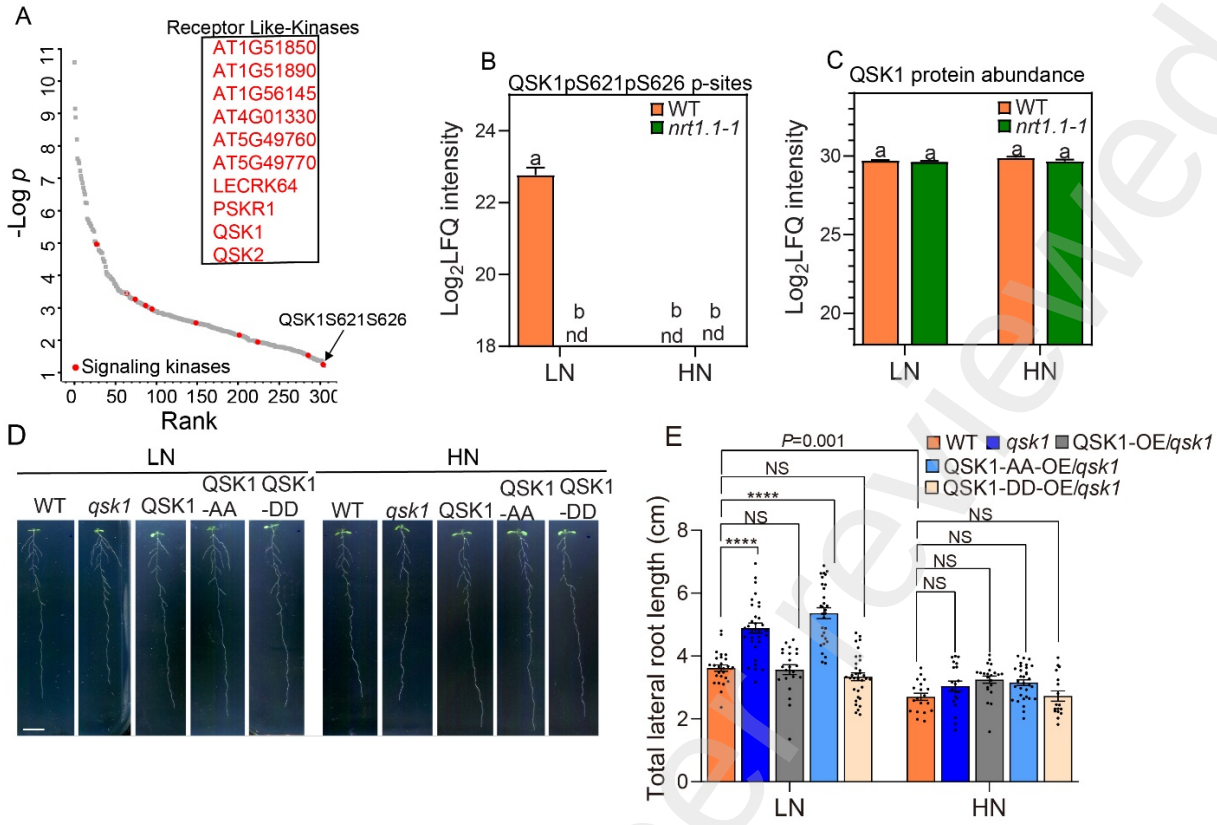

Figure 3. LN promotes NRT1.1-QSK1 interaction and QSK1 phosphorylation

(A) Ranking of phosphosites significantly upregulated in WT under LN and downregulated in *nrt1.1-1* in LN. 10 named receptor-like kinases are highlighted in red.

(B) Phosphorylation differences of S621/S626 on QSK1 in WT and *nrt1.1-1* induced by LN and HN.

(C) Differences of protein levels in QSK1 induced by LN and HN in WT and *nrt1.1-1*.

Data are mean + SD, at least 4 biological replicates (B-C), statistical analysis (B-C) was performed using Student *t*-test (different letter indicates $P<0.05$).

(D) Representative images of WT, *qsk1,* transgenic line overexpressing QSK1, QSK1 phospho-dead and as well as phosphorylation-mimic version in *qsk1* mutant (QSK1-OE/*qsk1,* QSK1-AA-OE/*qsk1* and QSK1-DD-OE/*qsk1*) in LN and HN medium, scale bar 1cm.

(E) Total lateral root length of WT, *qsk1*, QSK1-OE/*qsk1,* QSK1-AA-OE/*qsk1* and QSK1-DD-OE/*qsk1* in LN and HN medium. Bar plots indicate means ± SEM (at least 17 independent seedlings). Lateral roots were measured after 8 days on LN and HN. Statistical analysiswas performed using one-way ANOVA (****$P<0.0001$; NS, not significant).

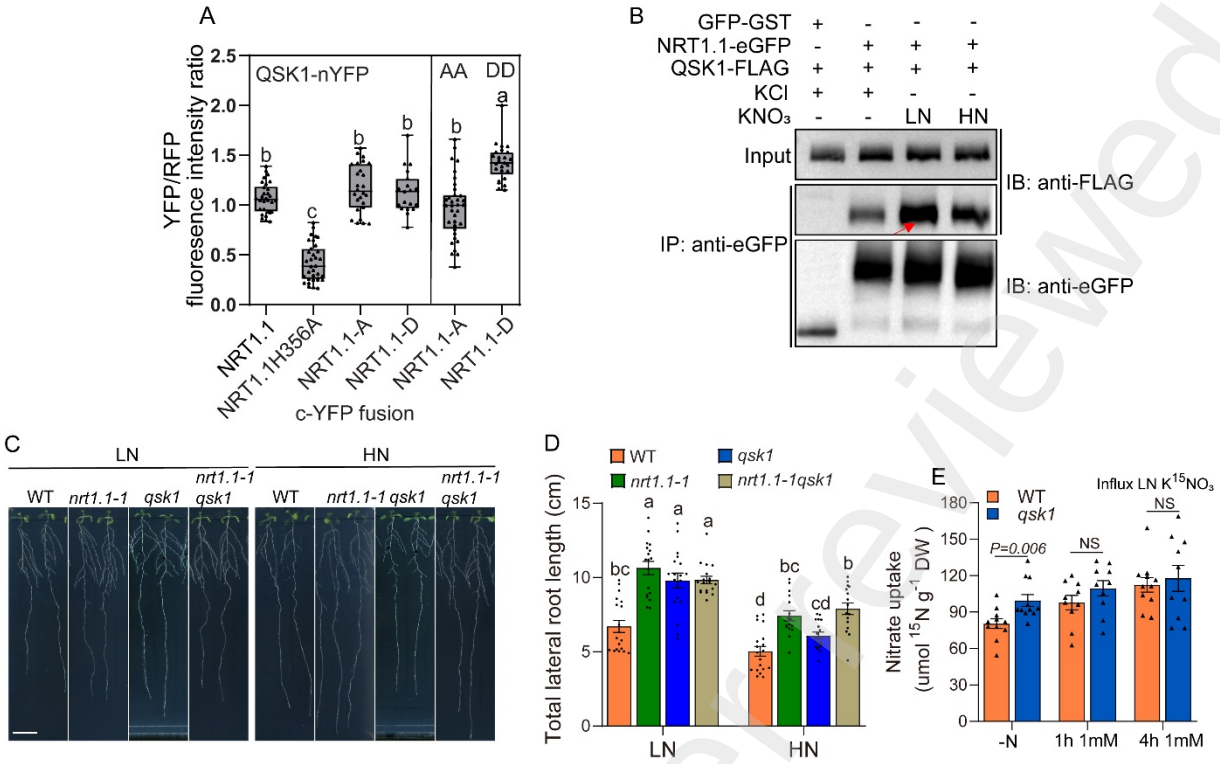

Figure 4. QSK1 functions downstream of NRT1.1 to modulate LRs growth in LN

(A) Quantification of the *in vivo* rBiFC interaction of QSK1, QSK1SASA, and QSK1SDSD with NRT1.1, NRT1.1H356A, NRT1.1T01A, and NRT1.1T01D. rBiFC calibration is shown in Figure S3. 18-35 randomly selected cells were quantified.

(B) Co-IP assays using membrane protein mixture extracted from tobacco leaves (*Nicotiana benthamiana*) expressing NRT1.1-eGFP and QSK1-FLAG in the presence of LN (0.45 mM KNO_3), HN (9.4 mM KNO_3) or potassium chloride (0.45 mM).

(C) Representative images of WT, *nrt1.1-1*, *qsk1* and *nrt1.1-1qsk1* in LN and HN medium, scale bar, 1cm. Different letters (A and D) represent significant differences at $p<0.05$ according to one-way ANOVA with a Tukey test.

(D) Total lateral root length of WT, *nrt1.1-1*, *qsk1*, and *nrt1.1-1qsk1* in LN and HN medium. Bar plots indicate means ± SEM (16-20 independent seedlings). Lateral roots were measured after 10 days on LN and HN medium.

Different letters (A and D) represent significant differences at $p<0.05$ according to one-way ANOVA with a Tukey test.

(E) ^{15}Nitrate uptake activity under LN. Bar plots indicate means ± SEM (at least 10 biological replicates). Statistical analysis was performed using two-tailed Student *t*-test ($P<0.05$; NS, not significant).

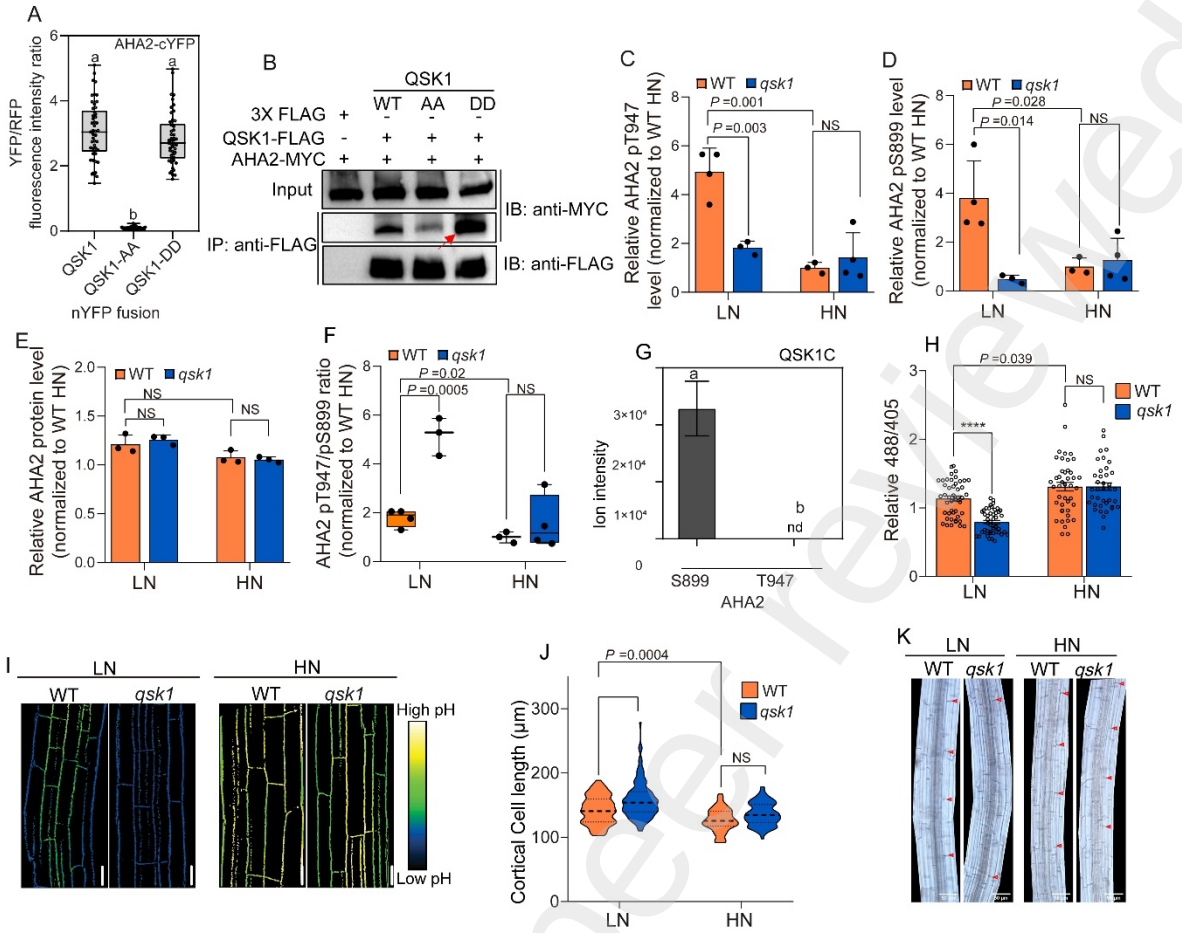

Figure 5. phosphorylated QSK1 forms a strong complex with AHA2 and represses proton pump activity in LN

(A) Quantification of the *in vivo* rBiFC interaction of QSK1, QSK1SASA and QSK1SDSD with AHA2. rBiFC calibration is shown in Figure S3. 50 randomly selected cells were quantified. Different letters represent significant differences at $p<0.05$ according to one-way ANOVA with a Tukey test.

(B) Co-IP assays using membrane protein mixture extracted from tobacco leaves (*Nicotiana benthamiana*) expressing QSK1-FLAG, QSK1-AA-FLAG and QSK1-DD-FLAG with AHA2-MYC.

(C and D) Difference of phosphorylation levels of T947 (C) and S899 (D) on AHA2 induced by LN and HN in WT and *qsk1*.

(E) Difference of protein levels of AHA2 under LN and HN in WT and *qsk1*.

(F) Box plots show T947/S899 phosphorylation ratio for WT and *qsk1* under LN. Center lines of boxes represent medians, vertical line indicates the minimal/maximal value.

Data (C, D and E) are mean+SD. Statistical analysis (C-F) was performed using two-tailed Student *t*-test (****$P<0.0001$; NS, not significant).

(G) *In vitro* peptide phosphorylation assay using GLDIETPSHY**T**V (covering T947) and EAVNIFPEKG**S**YR (covering S899) from AHA2 as substrates for the QSK1C terminus. nd indicates not detected.

(H and I) Quantification (H) and confocal images (I) of apoplastic pH in the lateral root EZ of WT and *qsk1* grown on LN and HN medium. Ratiometric value (488 nm/405 nm) of fluorescent

HPST was used to monitor pH in the EZ of lateral roots, n ≥ 39 individual root for each. For I, scale bar 20 μm.
(J and K) Quantification (J) and images (K) of cortical cell length of the lateral roots mature zone of WT and *qsk1* grown on LN and HN medium. n ≥ 61 cells for each. For K, scale bar 50 μm.
Statistical analysis (H and J) was performed using one-way ANOVA with a Tukey test (****P<0.0001; NS, not significant).

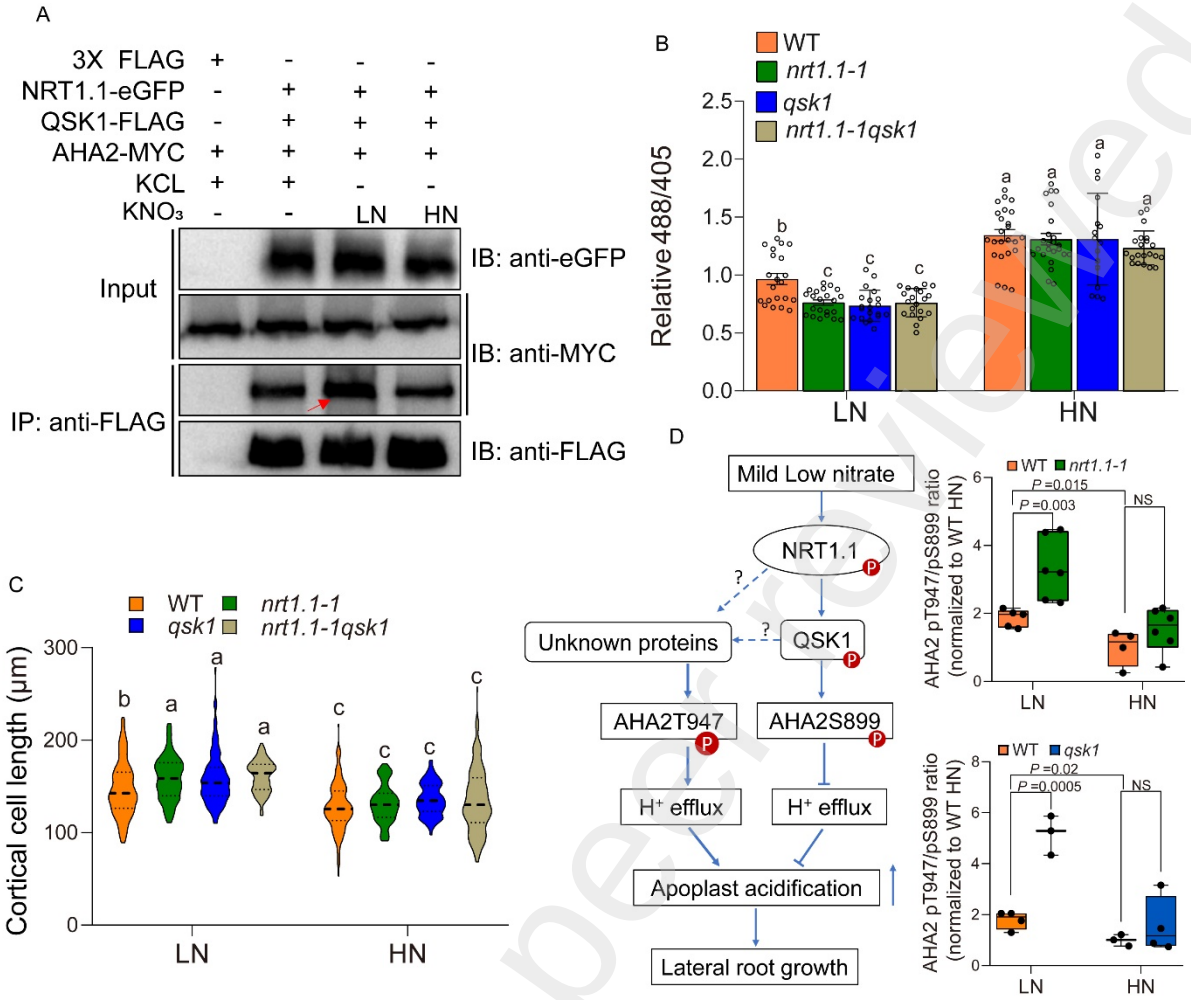

Figure 6. NRT1.1-QSK1 complex regulates AHA2 activity in LN

(A) Co-IP assays using membrane protein mixture extracted from tobacco leaves (*Nicotiana benthamiana*) expressing NRT1.1-eGFP, QSK1-FLAG and AHA2 in the presence of LN (0.45 mM KNO_3), HN (9.4 mM KNO_3) or potassium chloride (0.45 mM).

(B) Quantification of apoplastic pH in the lateral root EZ of WT, *nrt1.1-1*, *qsk1* and *nrt1.1-1qsk1* grown in LN and HN medium. Ratiometric value (488 nm/405 nm) of fluorescent HPST was used to monitor pH in the EZ of lateral roots, n≥16 individual root for each.

(C) Quantification of the cortical cell length of lateral roots mature zone of WT, *nrt1.1-1*, *qsk1* and *nrt1.1-1qsk1* grown on LN and HN medium, n≥152 cells for each.

Statistical analysis (B and C) was performed using one-way ANOVA with a Tukey test (****P<0.0001; NS, not significant).

(D) Proposed model for LN signal transduction through NRT1.1-QSK1 to AHA2. Perception of LN leads to NRT1.1 interacting with and phosphorylation of QSK1. Subsequently QSK1 recruits AHA2 and directly phosphorylates AHA2 at S899. NRT1.1 and QSK1 also induces AHA2T947 phosphorylation indirectly through unknown proteins (e.g. Kinases). As a result, phosphorylation ratio of T947/S899 and thus H^+-ATPase activity is affected. In both the *nrt1.1-1* and *qsk1* mutants, phosphorylation ratio of T947/S899 is dramatically increased due to a stronger reduction of phosphorylation at S899, resulting in an even higher proton activity, longer cells and longer LRs.